MODELING BRAIN LENTIVIRAL INFECTIONS DURING ANTIRETROVIRAL THERAPY IN AIDS

by

Weston Christopher Roda

A thesis submitted in partial fulfillment of the requirements for the degree of

Master of Science

in

Applied Mathematics

Department of Mathematical and Statistical Sciences
University of Alberta

Abstract

Understanding human immunodeficiency-1 (HIV-1) replication and latency in different reservoirs is an ongoing challenge in the care of patients with HIV/AIDS. A mathematical model was created that predicted HIV-1 and simian immunodeficiency virus (SIV) infection dynamics within the brain during effective combination antiretroviral therapy (cART). By developing a two compartment mathematical approach, a predictive model was generated from existing empiric data. Based on previous reports quantifying total viral DNA levels in brain from HIV-1 and SIV infections, estimates of proviral DNA burden were made, which were fit to a mathematical model predicting viral accrual in brain macrophages from primary infection. To our knowledge this is the first mathematical modeling study to quantify HIV-1 and SIV infection dynamics in the brain. Our modeling study indicates that HIV-1 and SIV provirus burdens in brain increase slowly over time. Assuming antiretroviral therapy suppresses HIV-1 infection outside the brain, an effective antiretroviral therapy could eradicate HIV-1 infection in the brain, albeit over a decade for patients without neurological complications and over two decades for those with HAND.

Preface

Part of the research completed in this thesis represents work performed in collaboration with three medical schools while studying towards a Master of Science degree at the University of Alberta from September 2014 to August 2016. The research collaboration included the following coauthors: Dr. Michael Y. Li and Mr. Michael S. Akinwumi at the Department of Mathematical and Statistical Sciences and Dr. Eugene L. Asahchop and Dr. Christopher Power at the Division of Neurology, Department of Medicine, at University of Alberta; Dr. Benjamin B. Gelman at the Texas NeuroAIDS Research Center and Department of Pathology at University of Texas Medical Branch; and Dr. Kenneth W. Witwer at the Department of Molecular and Comparative Pathobiology at John Hopkins University School of Medicine.

Acknowledgements

I would like to thank my family and friends for their support over the last two years while completing my MSc degree. I would like to express my deepest gratitude to my supervisor, Dr. Michael Li, for offering me this wonderful opportunity and for all of the help, encouragement, and guidance he has provided me with over the years. I would additionally like to thank all of the members of the Dr. Michael Li Lab. Special thanks to Michael Akinwumi for introducing me to the topic of HIV-1 brain infection that would motivate me to complete this thesis.

I am very grateful to my co-supervisor, Dr. Christopher Power, for all his insights and inspiration throughout the years. I would like to thank the entire Power Lab. Special thanks to Dr. Eugene Asahchop and Mr. William Branton for all of their help and advice during this research.

I would also like to thank the members of the thesis committee Dr. Yingfei Yi, Dr. Hao Wang, and Dr. James Muldowney for their time and help in the completion of this thesis.

I thank Dr. Benjamin Gelman and Dr. Kenneth Witwer for their collaboration, access to clinical and experimental data, and perceptive comments regarding this research. I would like to acknowledge Ms. Suzanne Queen for database assistance.

Finally, I would like to thank the Department of Mathematical and Statistical Sciences at University of Alberta for their generous financial support.

Table of Contents

List of Tables

List of Figures

Chapter 1

Introduction

Combination antiretroviral therapy (cART) has evolved over the past 20 years such that it is highly effective in suppressing human immunodeficiency virus-1 (HIV-1) replication in blood although recent data suggest that HIV-1 continues to replicate and replenish during cART in other tissues [1]. cART cannot eradicate latently infected cells and some organs in the human body are relatively inaccessible to cART. Moreover, some organs exert limited immune responses resulting in reservoirs of latently or productively infected cells [2]. Viral reservoirs represent a critical problem for the eradication of HIV-1 infection and the clinical care of HIV/AIDS [3].

The brain is a natural anatomical reservoir for HIV-1 infection [4]. The brain is devoid of in situ adaptive immune responses and the blood-brain barrier (BBB) restricts antiretroviral agents from entering the brain [5]. HIV-1 can reside indefinitely in brain cells and these infected cells support systemic brain infection [4, 6].

HIV-1 infection can lead to neurological disorders including HIV-associated neurocognitive disorder (HAND), which occurs in a subset of patients despite

effective viral suppression in blood accompanied by restoration of CD4+ T cell levels [7]. HIV-infected patients with HAND may have lower survival rates compared with HIV-infected patients without neurological disorders [7].

Although there is an increased appreciation and understanding of clinical aspects of HIV-1 brain infection, the underlying dynamics of viral replication and latency in the brain remain unclear. While mathematical modeling has been extensively used to study HIV-1 infection dynamics of cell populations in the blood (Section 1.A.1) and few modeling studies are related to HIV-1 infection in the central nervous system (CNS) (Section 1.B.1 and 1.B.2), to our knowledge this is the first mathematical modeling study to quantify HIV-1 and simian immunodeficiency virus (SIV) infection dynamics in the brain.

1.A Lentiviral infections in the blood and viral reservoirs

The immunodeficiency-associated lentiviruses including HIV-1, SIV, feline immunodeficiency virus (FIV), and bovine immunodeficiency virus (BIV) cause a prototypic disease pattern in the blood [8]. It begins with primary infection inducing acute disease accompanied by a robust immune response, which is followed by a long period of subclinical infection. The last phase of the disease is defined by profound immunosuppression and inflammation leading to AIDS, culminating in death [2]. The primary target cells for HIV-1 infection in the blood are CD4+ T cells [9]. HIV-1 infects other cells in the blood including cells of the monocyte/macrophage lineage [2]. While CD4+ T cells have a shortened lifespan after infection [9], monocytes and macrophages are

long-lived cells regardless of infection status [10, 11]. Target cells that contain integrated viral DNA but do not produce virus are called latently infected cells [9]. Latently infected cells have the capability to reinitiate virus replication and become productively infected cells [2, 9].

Though cART is very successful in suppressing HIV-1 replication in the blood, certain tissues have limited cART penetration and limited immune response and these tissues result in viral reservoirs with latently and productively infected cells [2]. HIV-1 virus can evade the immune system by residing inside anatomical viral reservoirs such as the brain [12]. Anatomical viral reservoirs like the brain present a crucial problem for the eradication of HIV-1 from infected individuals [5].

1.A.1 HIV-1 mathematical models in the blood

Mathematical models have been used extensively to study HIV-1 infection in the blood [13, 14, 9]. Two pioneers for using mathematical models to get a precise mathematical interpretation of HIV-1 blood viral decay data in 1995 were Alan Perelson and Martin Nowak [13, 14, 9]. An overview of previous HIV-1 mathematical models in the blood are presented in this section (1.A.1).

Basic model of HIV-1 infection in the blood

The earliest mathematical model of HIV-1 infection in the blood was developed by Alan Perelson and Martin Nowak [13, 14, 9]. It is a nonlinear autonomous ordinary differential equation (ODE) model with the following three compartments: susceptible CD4+ T cells, x; infected CD4+T cells, y; and free virus particles, v. It is assumed that the CD4+T cells are produced at a constant

rate λ and die at the rate k_x per cell. The free virus particles infect the susceptible CD4+T cells at a rate proportional to the product of their populations, βxv (the simple mass action infection term). The death rate of infected CD4+ T cells is k_y per cell, where $k_y > k_x$ to reflect the shortened lifespan of infected CD4+ T cells. Free virus particles are produced by infected CD4+ T cells at the rate p per cell. The death rate of free virus particles is a per virus. The ODE model is the following:

$$\begin{aligned} \frac{dx}{dt} &= \lambda - k_x x - \beta xv \\ \frac{dy}{dt} &= \beta xv - k_y y \\ \frac{dv}{dt} &= py - av. \end{aligned} \tag{1.1}$$

This model was able to describe the dynamics of acute HIV-1 infection in the blood but this model does not include factors such as antiretroviral therapy and latently infected cells [13].

Modeling HIV-1 infection with antiretroviral therapy in the blood

Reverse transcriptase inhibitors prevent the infection of susceptible CD4+ T cells by stopping the conversion of single-stranded HIV-1 RNA into double-stranded HIV-1 DNA [9]. The effectiveness of the reverse transcriptase inhibitors ϵ_{RTI} is included in the basic model of HIV-1 infection (1.1) [13, 9]:

$$\begin{aligned} \frac{dx}{dt} &= \lambda - k_x x - (1-\epsilon_{RTI})\beta xv \\ \frac{dy}{dt} &= (1-\epsilon_{RTI})\beta xv - k_y y \\ \frac{dv}{dt} &= py - av, \end{aligned} \tag{1.2}$$

where $0 \leq \epsilon_{RTI} \leq 1$ and $\epsilon_{RTI} = 1$ denotes 100% effectiveness of the reverse transcriptase inhibitors.

Protease inhibitors prevent infected CD4+ T cells from assembling new infectious virus particles [9]. The effectiveness of the protease inhibitors ϵ_{PI} is included in the previous model of HIV-1 infection by splitting the free virus particles into two different populations [9, 13]: non-infectious viral particles, v_{NI}, and infectious viral particles, v_I. The basic model of HIV-1 infection in the blood including both reverse transcriptase inhibitors and protease inhibitors is the following:

$$\begin{aligned} \frac{dx}{dt} &= \lambda - k_x x - (1 - \epsilon_{RTI})\beta x v \\ \frac{dy}{dt} &= (1 - \epsilon_{RTI})\beta x v - k_y y \\ \frac{dv_{NI}}{dt} &= (1 - \epsilon_{PI}) p y - a v_{NI} \\ \frac{dv_I}{dt} &= \epsilon_{PI} p y - a v_I, \end{aligned} \tag{1.3}$$

where $0 \leq \epsilon_{RTI} \leq 1$ and $0 \leq \epsilon_{PI} \leq 1$. This model was able to describe the dynamics of HIV-1 infection in the blood over the first two weeks of antiretroviral therapy but this model does not include latently infected cells [13].

Modeling HIV-1 infection with latency in the blood

When CD4+ T cells becomes infected, they can become different types of infected cells [9]. In this model, when CD4+ T cells becomes infected, they will either become productively infected cells with probability q_1, latently infected cells with probability q_2, and defective infected cells (harbor defective provirus)

with probability q_3 [9]. Latently infected CD4+ T cells y_2 can be reactivated to become virus producing CD4+ T cells y_1 at rate γ [9]. This adjusts the antiretroviral therapy model in the blood (1.3) to become the following:

$$\begin{aligned}
\frac{dx}{dt} &= \lambda - k_x x - (1-\epsilon_{RTI})\beta x v \\
\frac{dy_1}{dt} &= q_1(1-\epsilon_{RTI})\beta x v - k_{y_1} y_1 + \gamma y_2 \\
\frac{dy_2}{dt} &= q_2(1-\epsilon_{RTI})\beta x v - k_{y_2} y_2 - \gamma y_2 \\
\frac{dy_3}{dt} &= q_3(1-\epsilon_{RTI})\beta x v - k_{y_3} y_3 \\
\frac{dv_{NI}}{dt} &= (1-\epsilon_{PI}) p y_1 - a v_{NI} \\
\frac{dv_I}{dt} &= \epsilon_{PI} p y_1 - a v_I,
\end{aligned} \tag{1.4}$$

where $q_1 + q_2 + q_3 = 1$, $k_{y_1} \gg k_{y_2}, k_{y_3}$, and $a \gg k_{y_1} \gg k_{y_2} + \gamma$.

If the reverse transcriptase inhibitors and protease inhibitors are 100% effective ($\epsilon_{RTI} = 1$ and $\epsilon_{PI} = 1$), then in the model (1.4) the latently infected CD4+ T cells are responsible for the slower second phase of viral decay in the blood after the administration of reverse transcriptase inhibitors and protease inhibitors since $a \gg k_{y_1} \gg k_{y_2} + \gamma$ [9, 15].

The third phase of viral decay in the blood after the administration of treatment occurs when the HIV-1 RNA drops below 50 copies/mL [15]. This phase is characterized by episodes of viral increase above the limit of detection [15]. These viral episodes are termed viral blips [15]. In a modified version of model (1.4), it is hypothesized that these viral blips are caused by the antigenic stimulation of latently infected CD4+ T cells to activated CD4+ T cells [15].

Modeling HIV-1 infection with the macrophage population in the blood

In an early study, the macrophage population was incorporated into a version of the latently infected HIV-1 model in the blood (1.4) [10]. Here the variable m is the concentration of susceptible macrophages and m^* is the concentration of infected macrophages [10]:

$$\begin{aligned}
\frac{dx}{dt} &= \lambda - k_x x + rx\left(1 - \frac{x + y_1 + y_2}{T_{max}}\right) - (\beta_{v_x} xv + \beta_{m^*} xm^*) \\
\frac{dy_1}{dt} &= \gamma y_2 - k_{y_1} y_1 \\
\frac{dy_2}{dt} &= (\beta_{v_x} xv + \beta_{m^*} xm^*) - k_{y_2} y_2 - \gamma y_2 \\
\frac{dv}{dt} &= N k_{y_1} y_1 + pm^* - av - \beta_{v_x} xv \\
\frac{dm}{dt} &= k_m(s - m) - \beta_{v_m} mv \\
\frac{dm^*}{dt} &= \beta_{v_m} mv - k_{m^*} m^*.
\end{aligned} \tag{1.5}$$

The new parameters in the model are the following: r, the growth rate of CD4+ T cells; T_{max}, the carrying capacity of the total CD4+ T cell population; β_{v_x}, the HIV-1 transmission rate from free virus to susceptible CD4+ T cells; β_{m^*}, the HIV-1 transmission rate from infected macrophages to susceptible CD4+ T cells; β_{v_m},, the HIV-1 transmission rate from free virus to macrophages; N, the number of free virion produced per actively infected CD4+ T cell; p, the production of free virus from infected macrophages; s, the rate of production of susceptible macrophages.

This model (1.5) demonstrated a slower depletion of CD4+ T cells and

persistence of HIV-1 infection in the presence of a small number of free virus.

1.B Brain lentiviral reservoir

HIV-1 and SIV can be detected in brain tissue within weeks after primary infection [16, 17]. Evidence shows HIV-1 and SIV can enter the brain through trafficking infected macrophages [8, 18, 19]. Three cell types in the brain are known to be permissive to primate lentivirus infections: astrocytes, perivascular macrophages and microglia. Brain macrophages, including microglia and perivascular macrophages, display features of productive HIV-1 and SIV infections [9, 10]. In contrast, infected astrocytes contain viral genome but do not typically display features of active viral replication in vivo. The brain is relatively inaccessible to cART [5]. The brain also lacks an adaptive immune response [12]. HIV-1 has the potential to stay in brain macrophages for the lifetime of an infected patient and the brain is an important reservoir of HIV-1 [4].

HIV-related neurological disorders occur frequently for HIV-infected patients including patients on cART [7]. HIV-related neurological disorders majorly affect the completion of everyday activities and they can cause interference in the adherence to cART [20].

The underlying viral dynamics in the brain remain unclear. Cross-sectional autopsy studies of autopsied brain tissues revealed highly variable HIV-1 RNA levels in brain but the impact of combination antiretroviral therapy (cART) on brain viral burden remains uncertain, largely because of the relative inaccessibility of prospectively analyzed brain tissues.

A small number of earlier modeling studies are related to HIV-1 infection

in the CNS. These earlier studies are presented in the following two sections (Section 1.B.1 and 1.B.2). These earlier studies do not model the brain. Our new mathematical model quantifies HIV-1 and SIV infection dynamics in the brain and our model is presented in Chapter 3.

1.B.1 HIV-1 mathematical models related to central nervous system

Previous mathematical models have attempted to measure the dynamics of HIV-1 infection by modeling the three compartments of peripheral blood, lymph nodes, and the central nervous system (CNS) together [21, 22]. The migration of monocytes from the peripheral blood to the CNS was considered in the study mathematical model but the progression of the disease within the CNS was not modeled [21]. Another study created a model including the dynamics of uninfected monocytes, infected monocytes, uninfected macrophages, and infected macrophages in the CNS but the model specification in the CNS was unclear and the CNS dynamics were not fit to longitudinal CNS data [22].

A previous two compartment mathematical model in the CSF showed a strong relationship between the neurotoxin quinolinic acid (QUIN) released from activated macrophages and active CSF HIV infection [23]. The model included one compartment for QUIN in the plasma and the other compartment for QUIN in the CSF; this model did not include a compartment for macrophages [23].

Several mathematical models of cell-to-cell spread motivated from the biology of HIV-1 infection in tissue culture and brain tissue were fit to lymph node tissue culture data in vivo [24, 25, 26]. These mathematical models are

primarily two compartment models of cell-to-cell spread with delay [25, 26]. The following is a general model for the cell-to-cell spread of HIV-1 infection in tissue culture [25]:

$$\begin{aligned} \frac{dx}{dt} &= rx\left(1 - \frac{x+y}{M_x}\right) - \beta xy \\ \frac{dy}{dt} &= \alpha\left[\int_{-\infty}^{t} x(u)y(u)F(t-u)\,du\right] - \mu y, \end{aligned} \tag{1.6}$$

where x are the concentration of healthy cells, y are the concentration of infected cells, r is the effective reproductive rate of healthy cells, M_x is the effective carrying capacity of the system, β is the infection of healthy cells by the infected cells, $\frac{\alpha}{\beta}$ is the fraction of cells surviving the incubation period, μ is the death rate of infected cells, and productively infectious cells at time t were infected u time units ago with u distributed according to a probability distribution $F(u)$.

1.B.2 Statistical machine learning methods concerning HIV-1 infection in central nervous system

Support Vector Machines (SVM) produce nonlinear boundaries for data classification problems by constructing a linear boundary in a large transformed version of the feature space [27]. SVM methods have been applied to data from patients with advanced HIV-infection to determine the most important features that are associated with the presence of HIV-associated neurological disorders (HAND) or neuropsychological performance (NP)

[28, 29]. These features were the following: age, education level, duration of HIV infection, current haemoglobin level, current CD4 T-cell count, current

plasma $\log_10$ HIV RNA, current plasma viral detection, past CNS HIV-related diseases, cART CNS penetration effectiveness (CPE), depressive complaints, and duration of current cART [28, 29]. It was noted in the earlier study that the method of SVM is particularly difficult because the method tries to assess a neurological condition based on features that usually pertain to background data or data received from peripheral blood [28].

Statistical machine learning methods are also being considered to design future treatment schedules for patients [30].

1.C Objective and hypothesis

Objective

Our mathematical modeling study aimed to quantify lentiviral replication dynamics in the brain, especially among patients receiving cART. We collected and analyzed published data on HIV-1 and SIV brain infection from several studies. In a 2013 study, HIV-infected patient brain specimens from the National NeuroAIDS Tissue Consortium (NNTC) were examined for patients with advanced disease [31]. Published data from four SIV studies examining macaque brain tissues without cART [32, 33, 34, 35] were also included in our study. A mathematical model was formulated to describe HIV-1 and SIV infection dynamics in brain macrophages. The model was calibrated and validated using published brain data. The model showed HIV-1 and SIV infection in the brain progress slowly, due in large part to the long lifespan of infected brain macrophages. Indeed, the protracted turnover of infected brain macrophages might be an important hindrance in viral eradication [18]. Provided cART suppresses HIV-1 infection outside of the brain coupled with slow progression

of HIV-1 infection in the brain, moderately efficacious cART regimens could eradicate HIV-1 infection in the brain over years.

Hypothesis

Our hypothesis was that the brain macrophage population maintains HIV-1 infection of the brain and permits a progressive increase in integrated viral DNA burden that can be eradicated by efficient cART.

Chapter 2

Data

2.A HIV-1 brain-derived DNA data

When using autopsy data for brain tissue from human cohorts, there is minimal knowledge regarding duration of infection for each patient. It is widely accepted that approximately 10 years from primary infection a patient in the developed world will develop AIDS if untreated. From published studies of HIV-1 infection of the brain, we were able to ascertain data corresponding to two time points: 15 days after primary infection [16] and 10 years from primary infection [31].

Data used to estimate HIV-1 infected brain macrophages at primary infection for patients with and without neurological disorders came from a single patient study showing positive brain HIV-1 DNA detection 15 days after primary infection [16].

Brain tissue-derived data provided a large data set from HIV/AIDS patients with advanced disease (10 years from primary infection [31]) including data from patients ($n = 35$) without neurological disease as determined by the

NNTC neuropsychological test battery [31]; 73% of these patients were active on cART within 1 year of death. Brain-derived HIV-1 DNA data were also available from patients with HAND and/or encephalitis ($n = 22$); 62% were receiving cART within 1 year of death [31].

2.B SIV brain-derived DNA data

As each SIV study included brain-derived data corresponding to several time points, the four SIV studies were combined (32 macaques in total) to create a single longer time series of untreated SIV-infected brain tissue data (3, 10, 21, 56, and 84 days post-infection) [32, 33, 34, 35]. Data used for quantifying SIV-infected brain macrophages came from the brain viral DNA of this dataset. It was imperative to combine SIV studies where the macaques were the same species and each received the same strain and route of SIV infection. Three SIV studies used the same species of pigtailed macaques and were infected with the same viruses and input titers (SIV/DeltaB670/SIV/17E-Fr) [32, 33, 34, 35]. One SIV study used rhesus macaques; these macaques were infected with either SIVmac239 or SIVmac251 [35]. This latter study was included since it offered relevant data from the earliest time point (3 days post-infection).

2.C Biological data assumptions

The human brain contains an estimated 171 billion cells and approximately 84.6 billion glial cells [36]. A comprehensive study of the cellular composition of the grey matter of the human cerebral cortex indicated that microglia amount to only 5% of glial cells in grey matter [37]. From these analyses, the estimated

number of microglia in the human brain is 4.23 billion cells. Combining men and women, the approximate weight of a human brain is 1267 grams [38]. The projected number of microglia per gram of brain tissue is 3.34 million cells per gram. The number of susceptible brain macrophages was assumed to equal the total number of microglia. Each HIV- or SIV-infected brain macrophage can be assumed to contain a single copy of integrated viral DNA. Per gram of brain tissue, macaques have approximately the same number of susceptible brain macrophages as humans [36].

2.D Data conversion

The HIV-1 and SIV studies measuring viral DNA in brain tissues used different units for measuring viral DNA. Since each HIV- or SIV-infected brain macrophage is assumed to contain a single copy of integrated viral DNA, by converting total viral DNA to integrated viral DNA, we obtained the number of infected brain macrophages per gram of brain tissue. The conversion of the data is displayed in Table 2.1.

The HIV-1 brain viral DNA was measured in units of log10 HIV DNA copies + 200 per gram of brain tissue, where 200 represents the approximate threshold concentration of the assay from human brain specimens [31]. These data were converted to HIV DNA copies per gram of brain tissue by exponentiation. The ratio of integrated proviral DNA to total viral DNA is 1:86 [39] and this ratio was used to infer the number of integrated HIV DNA copies per gram of brain tissue.

For the four SIV studies, the SIV brain viral DNA was measured in two different units [32, 33, 34, 35]: log10 SIV DNA copy equivalents per 2 microgram

of total DNA and log10 SIV DNA copy equivalents per 10,000 cells.

For the former unit, this data was converted to SIV DNA copy equivalents per 2 microgram of total DNA by exponentiation. Using the conversion that each gram of brain tissue contains 4 micrograms of total host genomic DNA [40], the data was transformed to SIV DNA copy equivalents per gram of brain tissue. By using the ratio of integrated proviral DNA to total viral DNA (1:86) [39], the SIV DNA copy equivalents per gram of brain tissue were converted to integrated SIV DNA per gram of brain tissue.

For the latter unit, this data was converted to SIV DNA copy equivalents per 10,000 cells by exponentiation. Using the conversion that 150 000 cellular genomes contains 1 microgram of host genomic DNA [41], the data was transformed to SIV DNA copy equivalents per 1 microgram of host genomic DNA. By using the conversion that each gram of brain tissue contains 4 micrograms of host genomic DNA [40] and the ratio of integrated proviral DNA to total viral DNA (1:86) [39], the SIV DNA copy equivalents per 1 microgram of host genomic DNA was converted to integrated SIV DNA per gram of brain tissue.

Virus	Neurological disorders	Estimated years infected	Mean viral DNA copies/g	Estimated mean integrated viral DNA copies/g	Estimated mean infected brain macrophages/g	Ref
HIV-1	-	0.04	$9 - 172^{\alpha}$	$0.1 - 2^{\alpha}$	$0.1 - 2^{\alpha}$	[16]
HIV-1	No	≥ 10	1.95×10^3	23	23	[31]
HIV-1	Yes	≥ 10	9.88×10^4	1149	1149	[31]
SIV	-	0.008	0	0	0	[35]
SIV	-	0.008	0	0	0	[35]
SIV	-	0.027	1.41×10^3	16	16	[33]
SIV	-	0.058	1.24×10^3	14	14^{β}	[33]
SIV	-	0.058	6.22×10^3	72	72^{β}	[34]
SIV	17% with encephalitis	0.153	1.90×10^3	22	22	[33]
SIV	83% with encephalitis	0.230	3.22×10^4	375	375	[32]

Table 2.1: Conversion of HIV-1 and SIV DNA to the estimated mean number of infected brain macrophages per gram of brain tissue at different times from primary infection.

$^{\alpha}$This study detected proviral DNA in the brain by PCR. The number of viral DNA copies was not reported. It is assumed that the level of positive detection was approximately 100 copies Viral DNA per gram. The range of 9-172 copies Viral DNA per gram was chosen as the data from this study.
$^{\beta}$The six observations from each of these studies were combined and averaged giving 43 as the mean infected brain macrophages per gram at 0.058 years infected.

Chapter 3

The HIV-1 brain macrophage infection model

3.A Formulation of mathematical model

Experimental evidence shows HIV-1 and SIV can enter the brain through trafficking infected macrophages [8, 18, 19]. Three cell types in the brain are known to be susceptible to primate lentivirus infections: astrocytes, perivascular macrophages and microglia. Brain macrophages, including microglia and perivascular macrophages, display features of productive HIV-1 and SIV infections in the brain [9, 10]. Although astrocytes contain viral genome, astrocytes were not considered in this study because astrocytes have a limited infection and produce little or no virus in vivo [42].

A dynamic model was developed to quantify HIV-1 and SIV infection dynamics of brain macrophages. The brain macrophage population is divided into two compartments: susceptible brain macrophages, x, and infected brain macrophages, y. The infected brain macrophage population includes produc-

tively and latently infected brain macrophages. Given the limited viral RNA and DNA data it was necessary to combine productively and latently infected brain macrophages into a single population. HIV-1 and SIV infections of brain macrophages are assumed to spread principally through direct cell-to-cell interaction [18, 20]. Susceptible and infected brain macrophages are assumed to have homogeneous mixing and the brain macrophage population was assumed to be uniform throughout the brain. We followed an established method of modeling direct transmission between two populations by using the rate βxy as the number of new infections per unit time, where β is called the transmission coefficient. Without the presence of infection in the model, the number of susceptible brain macrophages converges to the equilibrium value of $\frac{\lambda}{k}$, where λ is the production rate of susceptible brain macrophages and k is the natural death rate for brain macrophages. Susceptible and infected brain macrophages were presumed to have the same death rate k because our group's earlier studies did not observe increased cellular death in HIV-infected versus uninfected brain macrophages [43]. In the HIV-1 dataset from the NNTC cohort, most patients were receiving cART within a year of death. We considered the percentage of cART effectiveness $\epsilon \times 100\%$, where $0 \leq \epsilon \leq 1$. The parameter ϵ is set to zero when there is no treatment.

The model is described by the set of nonlinear autonomous ordinary differential equations (ODEs):

$$\begin{aligned} \frac{dx}{dt} &= \lambda - kx - (1-\epsilon)\beta xy = \lambda - kx - \beta_\epsilon xy = h(x,y) \\ \frac{dy}{dt} &= (1-\epsilon)\beta xy - ky = \beta_\epsilon xy - ky = g(x,y), \end{aligned} \tag{3.1}$$

where $\beta_\epsilon = (1-\epsilon)\beta$. Given the initial conditions of the number of susceptible

brain macrophages x_0 and the number of infected brain macrophages y_0 at the time of initial infection, this model produces a temporal pattern of infected brain macrophage burden. Time units in this model are in years. Population units are the number of cells per gram of brain tissue.

Compared to mathematical models for HIV-1 infection in the plasma [9, 10], our model has a different transmission term. In the plasma and peripheral nervous system (PNS) infections occur by viral entry of host cell. In the brain, infections occur largely by direct cell-to-cell contact. For the same reason, unlike blood-based models for HIV-1 infection, our model does not include a compartment for free virus. Models with direct cell-to-cell transmission were used to describe the viral dynamics of HTLV-1 infection of CD4 T cells [9, 44, 45] whose lifespan is much shorter than brain macrophages. Mathematical models of HIV-1 infection of long-lived cells like macrophages were studied in [9] using virus-cell interaction as the mode of transmission.

3.B Vector differential equation form

The nonlinear autonomous ODE system (3.1) can be written as a *vector differential equation*:

$$\boldsymbol{x}' = \boldsymbol{f}(\boldsymbol{x}), \tag{3.2}$$

where $\boldsymbol{x} = \langle x, y \rangle$ and $\boldsymbol{f} = \langle h(x, y), g(x, y) \rangle$, with the vector of initial conditions $\boldsymbol{x}_0 = \langle x_0, y_0 \rangle$.

The *initial value problem* (IVP) that we would like to solve is the following:

Let E be an open set in $\mathbb{R}^2$. Assume that $\boldsymbol{f} \in C(E \to \mathbb{R}^2)$. Find a solution of the ODE model (3.1) in $\mathbb{R}^2$ which satisfies the initial condition, $\boldsymbol{x}_0$,

$$\begin{aligned} \boldsymbol{x}' &= \boldsymbol{f}(\boldsymbol{x}) \\ \boldsymbol{x}(t_0) &= \boldsymbol{x}_0. \end{aligned} \tag{3.3}$$

3.C Existence and uniqueness

In this section, we show that the initial value problem for the ODE model (3.3) has a unique solution given the vector of initial conditions $\boldsymbol{x}(t_0) = \boldsymbol{x}_0$ for some maximal interval of existence $t \in (\omega_-, \omega_+)$.

Definition (Lipschitz condition): Let E be an open subset of $\mathbb{R}^n$. Assume that $\boldsymbol{f} \in C(E \to \mathbb{R}^n)$. The function $\boldsymbol{f}$ satisfies the *Lipschitz condition* with respect to $\boldsymbol{x}$ if there exists constant K such that

$$|\boldsymbol{f}(t, \boldsymbol{x}_1) - \boldsymbol{f}(t, \boldsymbol{x}_2)| \leq K|\boldsymbol{x}_1 - \boldsymbol{x}_2| \tag{3.4}$$

for all $(t, \boldsymbol{x}_1), (t, \boldsymbol{x}_2) \in E$, where $|\cdot|$ is any norm in $\mathbb{R}^n$.

The functions $h(x, y)$ and $g(x, y)$ in the ODE model (3.1) are continuous and differentiable functions for all $|t| < \infty$, $|x| < \infty$, and $|y| < \infty$. Therefore, the function $\boldsymbol{f}$ is continuously differentiable for all $|t| < \infty$ and $|\boldsymbol{x}| < \infty$ and this implies that the function $\boldsymbol{f}$ is globally Lipschitz continuous over $\mathbb{R}^2$.

Theorem 3.1 (Existence-Uniqueness Theorem): *Let E be an open subset of $\mathbb{R}^n$ containing $\boldsymbol{x}_0$. Assume that $\boldsymbol{f} \in C(E \to \mathbb{R}^n)$ and $\boldsymbol{f}$ satisfies Lipschitz condition in E with respect to $\boldsymbol{x}$. Then there exists an $a > 0$ such that the initial value problem*

$$\begin{aligned} \boldsymbol{x}' &= \boldsymbol{f}(\boldsymbol{x}) \\ \boldsymbol{x}(t_0) &= \boldsymbol{x}_0 \end{aligned} \tag{3.5}$$

has a unique solution $\boldsymbol{\phi}(t)$ on the interval $t \in [t_0 - a, t_0 + a]$.

Theorem 3.2 (Maximal interval of existence): *Let E be an open subset of $\mathbb{R}^n$. Assume that $\boldsymbol{f} \in C(E \to \mathbb{R}^n)$ and $\boldsymbol{f}$ satisfies Lipschitz condition in E with respect to $\boldsymbol{x}$. Then for each point $\boldsymbol{x}_0 \in E$, there exists a maximal interval (ω_-, ω_+) on which the initial value problem* (3.5) *has a unique solution, $\boldsymbol{\phi}(t)$.*

Since the function $\boldsymbol{f}$ in the ODE model (3.1) is continuously differentiable for all $|t| < \infty$ and $|\boldsymbol{x}| < \infty$, then by theorem 3.1 there exists an $a > 0$ such that the initial value problem (3.3) has a unique solution $\boldsymbol{\phi}(t)$ on the interval $t \in [t_0 - a, t_0 + a]$. Furthermore, by theorem 3.2, a solution $\boldsymbol{\phi}(t)$ can be extended to its maximal interval of existence (ω_-, ω_+). If a solution $\boldsymbol{\phi}(t)$ stays in a compact subset of E during its maximal interval of existence, then it exists for $t \in (-\infty, \infty)$.

3.D Well-posedness

The ODE model (3.1) is considered well-posed if nonnegative initial conditions, x_0 and y_0, lead to nonnegative solutions, $x(t) \geq 0$ and $y(t) \geq 0$ for $t \geq 0$ - that is, the positive quadrant of $\mathbb{R}^2$

$$\mathbb{R}^2_+ = \{(x, y) \in \mathbb{R}^2 | x \geq 0, y \geq 0\} \tag{3.6}$$

is positively invariant with respect to (3.1).

To verify the positive invariance of $\mathbb{R}^2_+$ by showing that the direction of the vector field $\langle \lambda - kx - (1-\epsilon)\beta xy, (1-\epsilon)\beta xy - ky \rangle$ of (3.1) is either tangent to the coordinate or pointing into the interior of $\mathbb{R}^2_+$.

When $x = 0$,

$$\left.\frac{dx}{dt}\right|_{x=0} = \lambda > 0 \text{ and } \left.\frac{dy}{dt}\right|_{x=0} = -ky \leq 0.$$

Therefore, the vector field $\langle \lambda, -ky \rangle$ points into the interior of $\mathbb{R}^2_+$.

When $y = 0$,

$$\left.\frac{dx}{dt}\right|_{y=0} = \lambda - kx \text{ and } \left.\frac{dy}{dt}\right|_{y=0} = 0.$$

Since $\left.\frac{dy}{dt}\right|_{y=0} = 0$, the vector field $\langle \lambda - kx, 0 \rangle$ is tangent to the line $y = 0$. Also, this implies that solutions starting on the line $y = 0$ remain on the line. The line $y = 0$ is invariant.

Consequently, all solutions starting in $\mathbb{R}^2_+$ remain in $\mathbb{R}^2_+$ for $t > 0$.

3.E Feasible region

Let

$$G = \left\{ (x, y) \in \mathbb{R}^2_+ | x \leq \frac{\lambda}{k}, x + y \leq \frac{\lambda}{k} \right\}. \tag{3.7}$$

Theorem 3.3 shows that all solutions of the model (3.1) are bounded in the positively invariant set G. The set G is a feasible region for (3.1).

Theorem 3.3 (Feasible Region): *The set G defines a bounded feasible region for the ODE model* (3.1).

Proof. From the ODE model (3.1),

$$\frac{dx}{dt} = \lambda - kx - \beta_\epsilon xy \leq \lambda - kx \Rightarrow \limsup_{t\to\infty}(x(t)) \leq \frac{\lambda}{k}.$$

By adding the two equations in the ODE model (3.1), we receive

$$\frac{dx}{dt} + \frac{dy}{dt} = \lambda - kx - ky = \lambda - k(x + y)$$

$$\Rightarrow$$

$$\limsup_{t\to\infty}(x(t) + y(t)) = \frac{\lambda}{k}.$$

Now, to show all solutions starting in G for the ODE (3.1) remain in G for $t > 0$. Since all solutions of the ODE system (3.1) starting in $\mathbb{R}^2_+$ remain in $\mathbb{R}^2_+$ for $t > 0$, we need to show that when $x = \frac{\lambda}{k}$ and when $y = \frac{\lambda}{k} - x$ all

solutions remain in G for $t > 0$.

When $x = \frac{\lambda}{k}$,

$\left.\frac{dx}{dt}\right|_{x=\frac{\lambda}{k}} = \lambda - k\left(\frac{\lambda}{k}\right) = 0$ and $\left.\frac{dy}{dt}\right|_{x=\frac{\lambda}{k}} = \beta_\epsilon \frac{\lambda}{k} - ky.$

Since $\left.\frac{dx}{dt}\right|_{x=\frac{\lambda}{k}} = 0$, the vector field $\left\langle 0, \beta_\epsilon \frac{\lambda}{k} - ky \right\rangle$ is tangent to the line $x = \frac{\lambda}{k}$. Also, this implies that solutions starting on the line $x = \frac{\lambda}{k}$ remain on the line. The line $x = \frac{\lambda}{k}$ is invariant.

Now, when $y = \frac{\lambda}{k} - x$, the vector field is given by

$$\begin{bmatrix} \lambda - kx - \beta_\epsilon x \frac{\lambda}{k} + \beta_\epsilon x^2 \\ \beta_\epsilon x \frac{\lambda}{k} - \beta_\epsilon x^2 - \lambda + kx \end{bmatrix} = \left(\lambda - kx - \beta_\epsilon x \frac{\lambda}{k} + \beta_\epsilon x^2\right) \begin{bmatrix} 1 \\ -1 \end{bmatrix}.$$

This vector has slope -1 and it is parallel with the line $y = \frac{\lambda}{k} - x$. Therefore, this vector field is tangent to the line $y = \frac{\lambda}{k} - x$. This implies that solutions starting on the line $y = \frac{\lambda}{k} - x$ remain on the line. The line $y = \frac{\lambda}{k} - x$ is invariant.

Thus, we can consider a feasible region $G = \left\{(x, y) \in \mathbb{R}^2_+ | x \leq \frac{\lambda}{k}, x + y \leq \frac{\lambda}{k}\right\}$. The region G is positively invariant with respect to the model (3.1) and the model is well-posed. □

By theorem 3.3, the ω-limit sets of any initial point in $\mathbb{R}^2_+$ are contained in the closure of G, $\bar{G}$. When the limiting behavior of the solutions to the ODE model (3.1) are studied, it is sufficient to only consider solutions in the feasible region G.

3.F Basic and Control Reproduction Number

In a fully susceptible brain macrophage population without treatment, the average number of newly infected brain macrophages caused by a single infected brain macrophage during its infectious lifetime is given by the basic reproduction number, R_0:

$$R_0 = \frac{\beta\lambda}{k^2} \tag{3.8}$$

In a fully susceptible brain macrophage population with the presence of cART, the average number of newly infected brain macrophages caused by a single infected brain macrophage during its infectious lifetime is given by the control reproduction number, R_ϵ:

$$R_\epsilon = (1-\epsilon)\frac{\beta\lambda}{k^2} = \frac{\beta_\epsilon\lambda}{k^2} = (1-\epsilon)R_0 \tag{3.9}$$

where $\beta_\epsilon = (1-\epsilon)\beta$. The parameter ϵ represents the effectiveness of cART. The parameter ϵ is set to zero when there is no treatment.

The control reproduction number, R_ϵ, will be derived by considering the local stability of the disease-free equilibrium point P^0 in section 3.H.

3.G Equilibrium points

Theorem 3.4 (Existence of equilibria): 1. *If $R_\epsilon \leq 1$, then the disease-free equilibrium P^0 is the only equilibrium in the feasible region G.*

2. *If $R_\epsilon > 1$, then there exist two equilibria in the feasible region G: the disease-free equilibrium P^0 and the endemic equilibrium P^*.*

Proof. Equilibrium points occur when the ODE system (3.1) is set to 0:

$$\frac{dx}{dt} = \lambda - kx - (1-\epsilon)\beta xy = \lambda - kx - \beta_\epsilon xy = 0$$

$$\frac{dy}{dt} = (1-\epsilon)\beta xy - ky = \beta_\epsilon xy - ky = 0$$

$$\Rightarrow$$

$\lambda - kx - \beta_\epsilon xy = 0$ and $y(\beta_\epsilon x - k) = 0$.
This implies that either $y = 0$ or $x = \dfrac{k}{\beta_\epsilon}$.

When $y = 0$, we receive the disease-free equilibrium point

$$P^0(x^0, y^0) = \left(\frac{\lambda}{k}, 0\right).$$

When $x = \dfrac{k}{\beta_\epsilon}$, we receive the endemic equilibrium point

$$P^*(x^*, y^*) = \left(\frac{k}{\beta_\epsilon}, \frac{\lambda}{k} - \frac{k}{\beta_\epsilon}\right).$$

If $R_\epsilon \leq 1$, then $y^* = \dfrac{\lambda}{k} - \dfrac{k}{\beta_\epsilon} \leq 0$. Therefore, when $R_\epsilon \leq 1$, the only equilibrium in the feasible region G is the disease-free equilibrium P^0.

If $R_\epsilon > 1$, then $y^* = \dfrac{\lambda}{k} - \dfrac{k}{\beta_\epsilon} > 0$. Therefore, when $R_\epsilon \leq 1$, there exist two equilibria in the feasible region G: the disease-free equilibrium P^0 and the endemic equilibrium P^*.

□

3.H Local stability

The local behavior of the nonlinear ODE system (3.1) near a *hyperbolic equilibrium point* $\boldsymbol{x}^0$ is topologically equivalent to the local behavior of the following linear system [46]:

$$\boldsymbol{x}' = J(\boldsymbol{x}^0)\boldsymbol{x} \tag{3.10}$$

where J is the Jacobian matrix of the ODE system (3.1) and

$$J(x, y) = \begin{bmatrix} \frac{\partial h}{\partial x}(x, y) & \frac{\partial h}{\partial y}(x, y) \\ \frac{\partial g}{\partial x}(x, y) & \frac{\partial g}{\partial y}(x, y) \end{bmatrix} = \begin{bmatrix} -k - \beta_\epsilon y & -\beta_\epsilon x \\ \beta_\epsilon y & \beta_\epsilon x - k \end{bmatrix}. \tag{3.11}$$

Definition (Hyperbolic equilibrium point, [46]): An equilibrium point $\boldsymbol{x}^0$ is called a *hyperbolic equilibrium point* of the nonlinear autonomous ODE system (3.2) if none of the eigenvalues of the matrix $J(\boldsymbol{x}^0)$ have zero real part.

Definition (Types of equilibrium points, [46]): An equilibrium point $\boldsymbol{x}^0$ of (3.2) is called a *sink* if all of the eigenvalues of the matrix $J(\boldsymbol{x}^0)$ have negative real part; it is called a *source* if all eigenvalues of the matrix $J(\boldsymbol{x}^0)$ have positive real part; and it is called a *saddle* if it is a hyperbolic equilibrium point and the matrix $J(\boldsymbol{x}^0)$ has at least one eigenvalue with a positive real part and at least one with a negative real part.

The following theorem guarantees that any sink of (3.2) is uniformly asymptotically stable.

Theorem 3.5: *Suppose*

1. $\boldsymbol{f}(\boldsymbol{x}^0) = 0$
2. *The equilibrium point* $\boldsymbol{x}^0$ *is a sink.*

   Then the equilibrium point $\boldsymbol{x}^0$ *of the nonlinear autonomous ODE system* (3.2) *is uniformly asymptotically stable.*

Definition: The equilibrium point $\boldsymbol{x}^0$ is *unstable* if it is not stable.

Proposition 3.1 (Local stability of P^0): 1. *When* $R_\epsilon < 1$, *the disease-free equilibrium point* $P^0(x^0, y^0) = \left(\frac{\lambda}{k}, 0\right)$ *is locally asymptotically stable in the feasible region* G.

2. *When* $R_\epsilon > 1$, *the disease-free equilibrium point* $P^0(x^0, y^0) = \left(\frac{\lambda}{k}, 0\right)$ *is an unstable saddle point in the feasible region* G *and repels into the interior of the feasible region* G.

Proof. To study the local stability of the disease-free equilibrium point P^0, the point P^0 is plugged into the Jacobian matrix (3.11)

$$J(P^0) = \begin{bmatrix} \frac{\partial f}{\partial x}(P^0) & \frac{\partial f}{\partial y}(P^0) \\ \frac{\partial g}{\partial x}(P^0) & \frac{\partial g}{\partial y}(P^0) \end{bmatrix} = \begin{bmatrix} -k & -\beta_\epsilon \frac{\lambda}{k} \\ 0 & \beta_\epsilon \frac{\lambda}{k} - k \end{bmatrix} \tag{3.12}$$

.

Since the matrix (3.12) is upper triangular, the eigenvalues of the matrix (3.12) are $\theta_1 = -k$ and $\theta_2 = \beta_\epsilon \frac{\lambda}{k} - k$. The eigenvalue $\theta_1 < 0$ since $k > 0$. The disease-free equilibrium point P^0 is locally asymptotically stable if the eigenvalue $\theta_2 < 0$.

If $\theta_2 < 0$, then $\beta_\epsilon \frac{\lambda}{k} - k < 0 \Rightarrow \beta_\epsilon \lambda < k^2 \Rightarrow \frac{\beta_\epsilon \lambda}{k^2} < 1$.

Let $R_\epsilon = \frac{\beta_\epsilon \lambda}{k^2}$. (Note: This is a derivation of the control reproduction number, R_ϵ, by considering the local stability of the disease-free equilibrium point P^0.)

If $R_\epsilon < 1$, the disease-free equilibrium point P^0 is locally asymptotically stable.

If $R_\epsilon > 1$, the disease-free equilibrium point P^0 is a saddle point and unstable.

□

When $R_\epsilon = 1$, $\theta_2 = 0$ and the disease-free equilibrium P^0 is no longer a hyperbolic equilibrium. The method of linearization in not applicable when the equilibrium is not hyperbolic and the case of $R_\epsilon = 1$ will be covered using

the method of Lyapunov function in section 3.I.

The *Routh-Hurwitz criteria* will be used to prove the conditions for the local stability of the endemic equilibrium P^* (proposition 3.2).

Definition (Hurwitz matrix, [47]): Consider the real polynomial

$$P(s) = a_n s^n + a_{n-1} s^{n-1} + \cdots + a_0. \tag{3.13}$$

Consider the square $n \times n$ *Hurwitz matrix*

$$H = \begin{bmatrix} a_{n-1} & a_{n-3} & a_{n-5} & \dots & 0 \\ a_n & a_{n-2} & a_{n-4} & \dots & 0 \\ 0 & a_{n-1} & a_{n-3} & \dots & 0 \\ 0 & a_n & a_{n-2} & \dots & 0 \\ 0 & 0 & a_{n-1} & \dots & 0 \\ \vdots & \vdots & \vdots & & \vdots \\ 0 & 0 & 0 & \dots & a_0 \end{bmatrix}. \tag{3.14}$$

Definition (Hurwitz determinants, [47]): Let $D_1, \dots, D_n$ be the determinants of the principal minors of H (3.14).

Theorem 3.6 (Necessary and sufficient Routh-Hurwitz criteria, [48]): *If $a_n > 0$, then every zero of the real polynomial $P(s)$ (3.13) has negative real part if and only if the Hurwitz determinants D_k are all positive for $k = 1, \dots, n$.*

Corollary 3.6.1 (Routh-Hurwitz criteria for polynomials of degree 2): If $a_2 > 0$, then every zero of the real polynomial $P(s)$ (3.13) of degree 2 has negative real part if and only if $a_1 > 0$ and $a_0 > 0$.

Proof. Assume $a_2 > 0$. Consider the real polynomial

$$P(s) = a_2 s^2 + a_1 s + a_0.$$

Consider the square 2×2 Hurwitz matrix

$$H = \begin{bmatrix} a_1 & 0 \\ a_2 & a_0 \end{bmatrix}.$$

By theorem 3.6, every zero of the polynomial $P(s)$ has negative real part if and only if the *Hurwitz determinants* D_1 and D_2 are both positive. So, every zero of the polynomial $P(s)$ has negative real part if and only if $D_1 = a_1 > 0$ and $D_2 = a_1 a_0 > 0$. Therefore, every zero of the polynomial $P(s)$ has negative real part if and only if $a_1 > 0$ and $a_0 > 0$.

□

Now, the characteristic polynomial for determining the eigenvalues of a 2×2 Jacobian matrix (3.11) at an equilibrium point $\boldsymbol{x}^0$ is given by the following equation: $\det(J(\boldsymbol{x}^0) - \lambda I) = 0 \iff \lambda^2 - \mathrm{tr}(J(\boldsymbol{x}^0)) + \det(J(\boldsymbol{x}^0)) = 0$. Therefore, by corollary 3.6.1, every zero of the characteristic polynomial of degree 2 has negative real part if and only if $\mathrm{tr}(J(\boldsymbol{x}^0)) < 0$ and $\det(J(\boldsymbol{x}^0)) > 0$.

Proposition 3.2 (Local stability of P^*): 1. *When $R_\epsilon < 1$, the endemic equilibrium point $P^*(x^*, y^*) = (\frac{k}{\beta_\epsilon}, \frac{\lambda}{k} - \frac{k}{\beta_\epsilon})$ is an unstable equilibrium point in $\mathbb{R}^2$ outside of $\mathbb{R}^2_+$.*

2. *When $R_\epsilon > 1$, the endemic equilibrium point $P^*(x^*, y^*)$ is locally asymptotically stable in the feasible region G.*

Proof. To study the local stability of the endemic equilibrium point P^*, the point P^* is plugged into the Jacobian matrix (3.11)

$$J(P^*) = \begin{bmatrix} \frac{\partial f}{\partial x}(P^*) & \frac{\partial f}{\partial y}(P^*) \\ \frac{\partial g}{\partial x}(P^*) & \frac{\partial g}{\partial y}(P^*) \end{bmatrix} = \begin{bmatrix} -k - \beta_\epsilon y^* & -\beta_\epsilon x^* \\ \beta_\epsilon y^* & \beta_\epsilon x^* - k \end{bmatrix}. \tag{3.15}$$

By the *Routh-Hurwitz criteria*, all eigenvalues of a 2×2 matrix A have negative real parts if and only if $\mathrm{tr}(A) < 0$ and $\det(A) > 0$. Now,

$$\begin{aligned} \mathrm{tr}(J(P^*)) &= -k - \beta_\epsilon y^* + \beta_\epsilon x^* - k \\ &= -\beta_\epsilon \left(\frac{\lambda}{k} - \frac{k}{\beta_\epsilon} \right) + \beta_\epsilon \left(\frac{k}{\beta_\epsilon} \right) - 2k \\ &= \frac{-\beta_\epsilon \lambda}{k}. \end{aligned} \tag{3.16}$$

Since $0 \leq \epsilon \leq 1$, $\beta > 0$, $\lambda > 0$, and $k > 0$, then $\mathrm{tr}(J(P^*)) < 0$.

So,

$$\begin{aligned}\det(J(P^*)) &= (-k-\beta_\epsilon y^*)(\beta_\epsilon x^* - k) - (-\beta_\epsilon x^*)(\beta_\epsilon y^*) \\ &= -k\beta_\epsilon x^* + k^2 + \beta_\epsilon y^* k \\ &= \beta_\epsilon y^* k \\ &= \beta_\epsilon \lambda - k^2 \\ &= k^2(R_\epsilon - 1)\end{aligned} \tag{3.17}$$

If $R_\epsilon > 1$, then $det(J(P^*)) > 0$. Since $tr(J(P^*)) < 0$ and $det(J(P^*)) > 0$, P^* is locally asymptotically stable in the feasible region G.

If $R_\epsilon < 1$, then $det(J(P^*)) < 0$. Since $tr(J(P^*)) < 0$ and $det(J(P^*)) < 0$, P^* is unstable in $\mathbb{R}^2$ outside of $\mathbb{R}^2_+$.

□

3.I Global stability

To prove the global stability of P^0 and P^* we will use *Bendixson's criteria*, *Dulac's criteria*, and the *Poincaré-Bendixson Theorem*.

Theorem 3.7 (Bendixson's criteria, [46]): *Let $E \subset \mathbb{R}^2$ be a simply connected region. If*

$$\operatorname{div}(\boldsymbol{f}(\boldsymbol{x})) < 0 \tag{3.18}$$

(or > 0) for all $\boldsymbol{x} \in E$, then (3.2) *has no closed orbit lying entirely in E.*

Theorem 3.8 (Dulac's criteria, [46]): *Let $E \subset \mathbb{R}^2$ be a simply connected region. If there exists a scaler function $\alpha(\boldsymbol{x})$ such that*

$$\operatorname{div}(\alpha(\boldsymbol{x})\boldsymbol{f}(\boldsymbol{x})) < 0 \tag{3.19}$$

(or > 0) for all $\boldsymbol{x} \in E$, then (3.2) has no closed orbit lying entirely in E.

Theorem 3.9 (Poincaré-Bendixson Theorem): *Assume that $\mathbb{R}^2$. Let γ be a nonempty compact limit set of (3.2). If γ contains no equilibria, then γ is a periodic orbit.*

Theorem 3.10 (Global stability of P^0 and P^*):1. *If $R_\epsilon \leq 1$, then the disease-free equilibrium P^0 is the only equilibrium in the feasible region G and it is globally stable in this region.*

2. *If $R_\epsilon > 1$, then the disease-free equilibrium P^0 is unstable and the endemic equilibrium P^* is globally stable in the interior of the feasible region G.*

Proof. Consider the Lyapunov function

$$L(x, y) = y. \tag{3.20}$$

Then

$$\begin{aligned} L^* = \frac{dL}{dt} &= \frac{dy}{dt} \\ &= \beta_\epsilon xy - ky \\ &= y(\beta_\epsilon x - k) \\ &= \frac{k^2 y}{\lambda}(R_\epsilon x - \frac{\lambda}{k}). \end{aligned}$$

Assume that $R_\epsilon \leq 1$. Then

$$L^* \leq \frac{k^2 y}{\lambda}(x - \frac{\lambda}{k}) \leq 0,$$

provided that $R_\epsilon \leq 1$ and since $0 \leq x \leq \frac{\lambda}{k}$.

Let

$$\gamma = \{(x, y) \in G | \frac{dL}{dt} = 0\}. \tag{3.21}$$

A point is in the set γ if and only if $y = 0$ or $R_\epsilon = 1$ and $x = \frac{\lambda}{k}$.

By LaSalle's Invariance Principle, all limit points of solutions belong to the largest invariant set in γ.

If $R_\epsilon = 1$ and $x = \frac{\lambda}{k}$, then necessarily we have $x = \frac{\lambda}{k}$ and $y = 0$.

If $y = 0$, any solution of the model will stay in the set where $y = 0$ and $\frac{dx}{dt} = \lambda - kx$, and consequently $x(t) = \frac{\lambda}{k} + Ce^{-kt} \to \frac{\lambda}{k}$ as $t \to \infty$, where C is a constant.

In both these cases the only compact invariant set in the set γ is $\{P^0\}$. Therefore, all solutions in G converge to P^0.

Assume that $R_\epsilon > 1$. Then

$L^* > 0$ for all points $(x, y) \in G$ and P^0 is an unstable, saddle equilibrium and repels into the interior of the feasible region G.

Now, to show that when $R_\epsilon > 1$, the endemic equilibrium P^* is globally stable in the interior of the feasible region G. Use the Dulac multiplier $\alpha(x, y) = \frac{1}{y}$. Then

$$\frac{\partial}{\partial x}(\alpha h(x,y)) + \frac{\partial}{\partial y}(\alpha g(x,y)) = \frac{\partial(\frac{h}{y})}{\partial x} + \frac{\partial(\frac{g}{y})}{\partial y} = -\frac{k}{y} - \beta_\epsilon < 0 \qquad (3.22)$$

for all points (x, y) in the interior of G. Therefore, no periodic solutions can exist. By the Poincare-Bendixson Theorem, all solutions with initial condition in the interior of the feasible region G must have P^* as an ω-limit point. Since P^* is locally asymptotically stable, solutions that get close to P^* must converge to P^* and all ω-limit sets in the interior of G are equal to the singleton $\{P^*\}$. Therefore, P^* is globally stable in the interior of the feasible region G when $R_\epsilon > 1$.

□

Chapter 4

Numerical fitting

Brain macrophage death rate k was estimated directly from the cellular lifespan. The equilibrium population $\frac{\lambda}{k}$ of susceptible brain macrophages was fitted to the per gram amount of the brain microphages to obtain estimation of influx λ of susceptible brain macrophages (Table 4.1).

The transmission coefficient with cART regimen effectiveness ϵ, β_ϵ, and the initial population, y_0, of infected brain macrophages at initial infection, cannot be estimated directly from the available data. These were assessed by fitting the model predictions to the estimated per-gram numbers of infected brain macrophages at the time points in Table 2.1.

The method of Bayesian inference was implemented for the model fitting and is described in the following sections.

4.A Bayesian inference

HIV-1 DNA has been detected by PCR in the brain 15 days after exposure to the virus [16]. Based on the data in [16], we inferred that the range of mean

Symbol	Parameter	Estimate	Unit	Ref
x_0	Equilibrium number of susceptible brain macrophages	3.34×10^6	per g	[36, 37, 38]
λ	Influx of susceptible brain macrophages	6.68×10^6	per year	[37]
k	Death rate of brain macrophages	2	per year	[10]

Table 4.1: Parameters estimated from literature for both humans and macaques.

integrated viral DNA copies per gram is 0.1-2 with a uniform distribution at the initial HIV-1 brain infection, namely, $y_0 \sim$ U(0.1, 2). For SIV infected macaques, a simple linear regression model was fit to all SIV data to determine the range for the initial population, y_0, of SIV infected brain macrophages. The intercept from the regression has a 95% confidence interval of (-17.92, 90.19) and a uniform distribution was chosen for y_0, namely, $y_0 \sim$ U(0, 90.19).

The parameter for cART regimen effectiveness in brain, ϵ, was set to zero during the model fitting for the untreated SIV-infected macaque data. The parameter for cART regimen effectiveness in brain, ϵ, cannot be estimated from the literature for cART-treated HIV-infected patients. During the model fitting for the cART-treated HIV-infected patient data the parameter ϵ was set to $\bar{\epsilon}$ where $\bar{\epsilon}$ represented some unknown value in the possible range 0-1. This allowed the model fitting to form parameter estimates for the three different cohorts (Table 2.1): cART-treated HIV-infected patients without neurological disorders, cART-treated HIV-infected patients with neurological disorders, and untreated SIV-infected macaques.

Bayesian inference is used to fit the ODE model to the estimated number of infected brain macrophages at the time points in Table 2.1.

The ODE model was solved numerically by using the MATLAB function ode45 [49]. The function ode45 is based on an explicit Runge-Kutta (4,5) formula. The fitting was completed using a Markov Chain Monte Carlo (MCMC) sampling program from the MATLAB Central File Exchange [50]. The MCMC program sampled from the natural logarithm of the following unnormalized posterior distribution, $\pi(\boldsymbol{\theta}|D)$:

$$\pi(\boldsymbol{\theta}|D) = L(\boldsymbol{\theta}|D) \times P(\boldsymbol{\theta}) \tag{4.1}$$

where $\boldsymbol{\theta}$ is a vector of the unknowns β and y_0, $D = \{(t_1, d_1), \ldots, (t_n, d_n)\}$ is the observed data from Table 2.1, $L(\boldsymbol{\theta}|D)$ is the likelihood function, and $P(\boldsymbol{\theta}) = P(\beta) \times P(y_0)$ is the prior distribution with $\beta_\epsilon \sim$ U(a, b), $y_0 \sim$ U(c, d), and a, b, c, d are constants.

4.A.1 Non-homogeneous Poisson Process

The number of events during a time interval of length t is a Poisson random variable with parameter μt. The expected number of events during any such time interval is then μt. The expected number of events during a unit interval of time is μ.

We assume that the infected brain macrophages are distributed randomly and uniformly throughout the brain with an average of $\mu(\boldsymbol{\theta}, t)$ per unit gram of brain tissue, where $\mu(\boldsymbol{\theta}, t) = y(\boldsymbol{\theta}, t)$ is the solution to the ODE $\dfrac{dy}{dt}$ in the ODE model (3.1) fitted to the observed data in Table 2.1.

This is a non-homogeneous Poisson Process because the rate of occurrence μ is not constant over time [51].

Using this assumption of a non-homogeneous Poisson Process, the likelihood function is the following:

$$L(\boldsymbol{\theta}|D) = \prod_{i=1}^{n} \frac{\mu(\boldsymbol{\theta}, t_i)^{d_i} e^{-\mu(\boldsymbol{\theta}, t_i)}}{d_i!}, \tag{4.2}$$

where $\mu(\boldsymbol{\theta}, t_i) = y(\boldsymbol{\theta}, t_i)$ is the numerical solution to the ODE $\frac{dy}{dt}$ in the ODE model (3.1) at t_i fitted to the observed data in Table 2.1.

The likelihood function is the probability of the n observed counts $d_1, \ldots, d_n$ each independently Poisson distributed with means $\mu(\boldsymbol{\theta}, t_1), \ldots, \mu(\boldsymbol{\theta}, t_n)$.

4.A.2 Bayesian approach to ODE model fitting with Gaussian noise

This section introduces a method to fit an ODE model that assumes Gaussian noise instead of the Poisson distribution assumption. This fitting method assumes that the observed data $d_1, \ldots, d_n$ deviate from the solution to the ODE model $\mu(\boldsymbol{\theta}, t) = x(\boldsymbol{\theta}, t)$ by additive errors r that are independent and identically distributed Normal random variables with mean zero and variance σ^2:

$$d_i = x(\boldsymbol{\theta}, t_i) + r, \tag{4.3}$$

where $r \sim \mathrm{N}(0, \sigma^2)$.

The likelihood function is then given by the following equation:

$$L(\boldsymbol{\theta}|D) = \prod_{i=1}^{n} \frac{1}{\sqrt{2\pi}\sigma} e^{-\frac{(d_i - x(\boldsymbol{\theta}, t_i))^2}{2\sigma^2}}. \tag{4.4}$$

This likelihood function is commonly used for the Bayesian analysis of standard regression models with Gaussian noise [52] but this likelihood function has also been successfully used for the Bayesian analysis of mathematical models [53].

The variance σ^2 of the errors can be estimated by the variance of the observed data, by the variance of the errors for a regression fit to the observed data, or by the variance of the errors between a representative continuous curve and the observed data [53].

Furthermore, suppose there are m independent data sets that give information about the same vector of parameters $\boldsymbol{\theta}$ and for each j^{th} data set there is a specific ODE model solution $\mu_j(\boldsymbol{\theta}, t) = x_j(\boldsymbol{\theta}, t)$ to fit to the j^{th} data set. In this situation, the ODE model fitting with Gaussian noise would appear as the following: for $1 \leq j \leq m$,

$$d_i = x_j(\boldsymbol{\theta}, t_i) + r_j, \tag{4.5}$$

where $r_j \sim \mathrm{N}(0, \sigma_j^2)$ and $1 \leq i \leq n_j$.

If m independent data sets give information about the same vector of parameters $\boldsymbol{\theta}$, then the overall likelihood $L(\boldsymbol{\theta}|D_1, \ldots, D_m)$ of the combined m independent data sets is obtained by multiplying the m likelihood functions $L(\boldsymbol{\theta}|D_1), \ldots, L(\boldsymbol{\theta}|D_m)$ of $\boldsymbol{\theta}$ together [54]:

$$L(\boldsymbol{\theta}|D_1,\ldots,D_m) = L(\boldsymbol{\theta}|D_1)\cdot\ldots\cdot L(\boldsymbol{\theta}|D_m). \tag{4.6}$$

Using the likelihood function given by the Gaussian noise (4.4), if m independent data sets give information about the same vector of parameters $\boldsymbol{\theta}$ and for each j^{th} data set there is a specific ODE model solution $\mu_j(\boldsymbol{\theta},t) = x_j(\boldsymbol{\theta},t)$ to fit to the j^{th} data set, then the overall likelihood $L(\boldsymbol{\theta}|D_1,\ldots,D_m)$ is given by the following equation:

$$L(\boldsymbol{\theta}|D_1,\ldots,D_m) = \prod_{j=1}^{m}\prod_{i=1}^{n_j}\left(\frac{1}{\sqrt{2\pi}}\right)^m \frac{1}{\sigma_j} e^{-\dfrac{(d_i - x_j(\boldsymbol{\theta},t_i))^2}{2\sigma_j^2}}. \tag{4.7}$$

Considering the same situation as above except combining m correlated data sets that give information about the same vector of parameters $\boldsymbol{\theta}$, then the overall likelihood $L(\boldsymbol{\theta}|D_1,\ldots,D_m)$ is given by the following equation [55]:

$$L(\boldsymbol{\theta}|D_1,\ldots,D_m) = \left(\frac{1}{\sqrt{2\pi}}\right)^m \frac{1}{\sqrt{\det(C)}} e^{-\frac{1}{2}(\boldsymbol{y})^{\mathrm{T}} C^{-1}(\boldsymbol{y})}, \tag{4.8}$$

where $\boldsymbol{y} = (\boldsymbol{y}^1,\cdots,\boldsymbol{y}^n)^T$, $y_i^j = d_i - x_j(\boldsymbol{\theta},t_i)$ for $i \in \{1,\ldots,n_j\}$, and $C = \{\langle \boldsymbol{y}^w, \boldsymbol{y}^k\rangle\}$ with the auto- or cross-correlation between the vectors $\boldsymbol{y}^w$ and $\boldsymbol{y}^k$ given by $\langle \boldsymbol{y}^w, \boldsymbol{y}^k\rangle$. This likelihood equation (4.8) gives each data set equal weight [55].

In future studies, the likelihood function (4.8) could be used to fit a more complex ODE model to several different data sets during HIV and SIV infection in the brain.

4.B Markov Chain Monte Carlo sampler

When fitting the ODE model (3.1) to the untreated SIV-infected macaques data and the cART-treated HIV-infected patients without neurological disorders data, 4 chains with a total number of samples of 880,000 were used. Every 10^{th} sample was thinned from each chain and a burn in of 2,000 samples was removed from each chain. This left 20,000 actual samples for each chain returned from the MCMC method. The samples from each chain were consolidated giving a total of 80,000 samples.

When fitting the ODE model (3.1) to the cART-treated HIV-infected patients with neurological disorders data, a greater number of samples were needed to reach convergence of the MCMC sampling and 4 chains with a total number of samples of 1,760,000 were used.

Convergence to the posterior distribution

A sequence of random variables X_n **converges to the distribution** of X_∞ if their distribution functions $F_n(x) = P(X_n \leq x)$ **converge weakly** to F, the distribution of X_∞. [56]. The samples from the MCMC provide a sample path. It is important to diagnose if this sample path produces a sample from the target posterior distribution - that is, the sample path converges to the target posterior distribution. From the plot of the sample path, it is critical to find that the sample path has arrived at a stationary process and the sample path covers the domain of the target posterior distribution.

The pooled sample path for each estimated parameter are displayed in Figures 4.1, 4.2, 4.3, 4.4, 4.5, and 4.6. Each sample path shows that the pooled samples are oscillating very fast and displays no apparent trend indicating

that the sample path has arrived at a stationary process. By observing the unnormalized posterior distribution for each estimated parameter in section 4.C.1, it is seen that the sample path covers the domain of the target posterior distribution.

A formalized test of the convergence of the MCMC sampling to the estimated posterior distribution for each parameter was determined by using a general univariate comparison method [57]. The general univariate comparison method uses the distance of the empirical $100(1-\alpha)\%$ interval for the pooled samples, S, and divides this distance by the average of the distances of the empirical $100(1-\alpha)\%$ interval for each of the n chains, s_i, to receive the potential scale reduction factor, r [57]:

$$r = \frac{S}{\sum_{i=1}^{n} \frac{s_i}{n}}. \tag{4.9}$$

For the general univariate comparison method the empirical 95% interval was used. The potential scale reduction factor, r, was close to 1 for all the estimated parameters and this indicates that the MCMC sampling converged to the estimated posterior distribution for each parameter (Table 4.2).

Datasets	Ratio, r, for β	Ratio, r, for y_0
HIV-1 without neurological disorders	1.0002	0.9996
HIV-1 with neurological disorders	0.9969	0.9976
SIV untreated	0.9990	0.9986

Table 4.2: Potential scale reduction factor, r, for the model fit to three datasets.

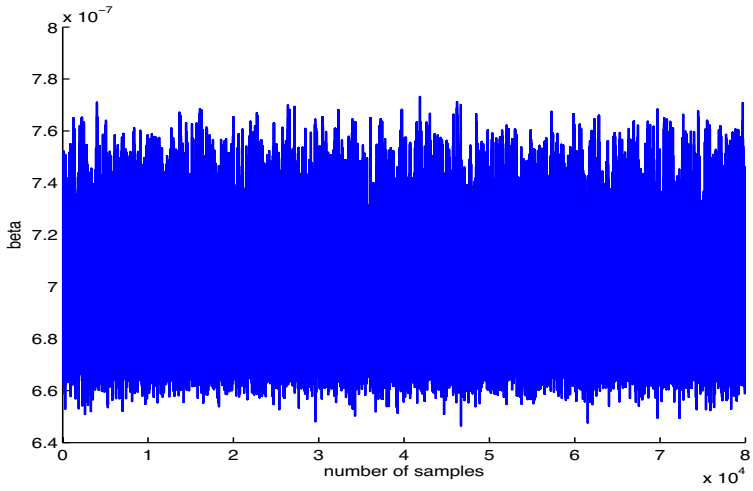

Figure 4.1: Chains convergent for HIV model parameter β for cART-treated patients without neurological disorders

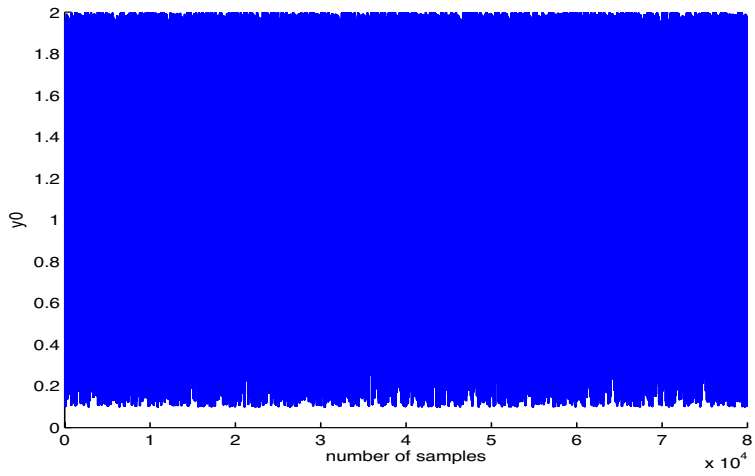

Figure 4.2: Chains convergent for HIV model parameter y_0 for cART-treated patients without neurological disorders

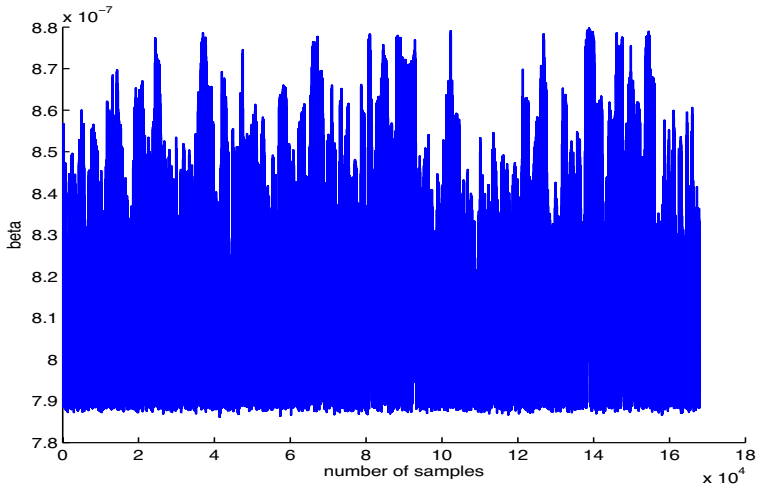

Figure 4.3: Chains convergent for HIV model parameter β for cART-treated patients with neurological disorders

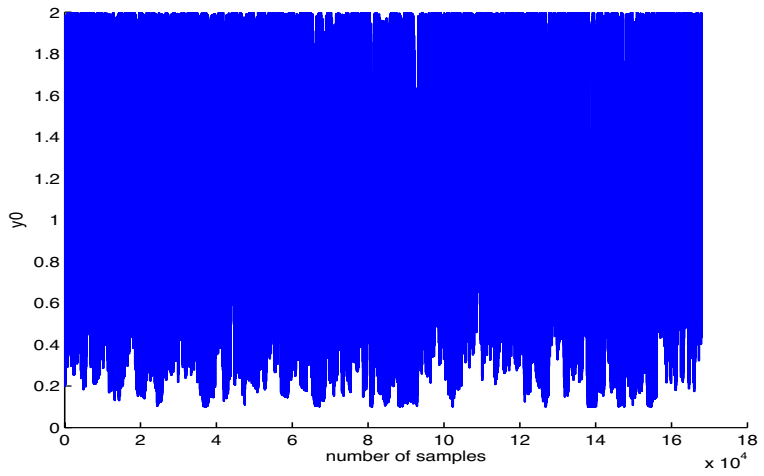

Figure 4.4: Chains convergent for HIV model parameter y_0 for cART-treated patients with neurological disorders

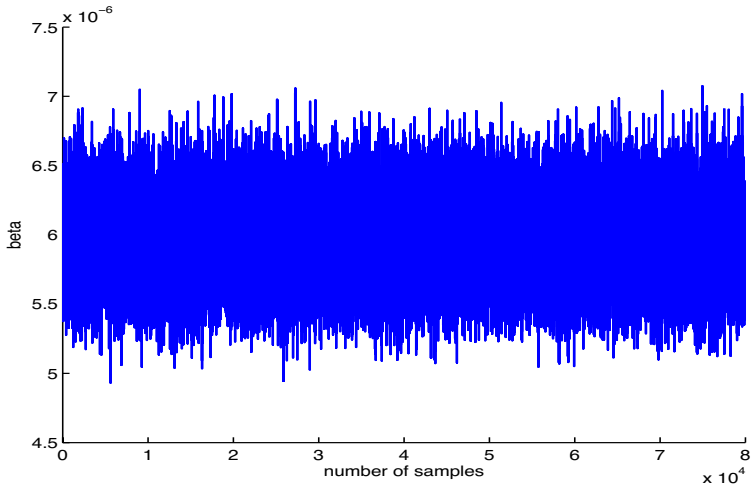

Figure 4.5: Chains convergent for SIV model parameter β for untreated macaques

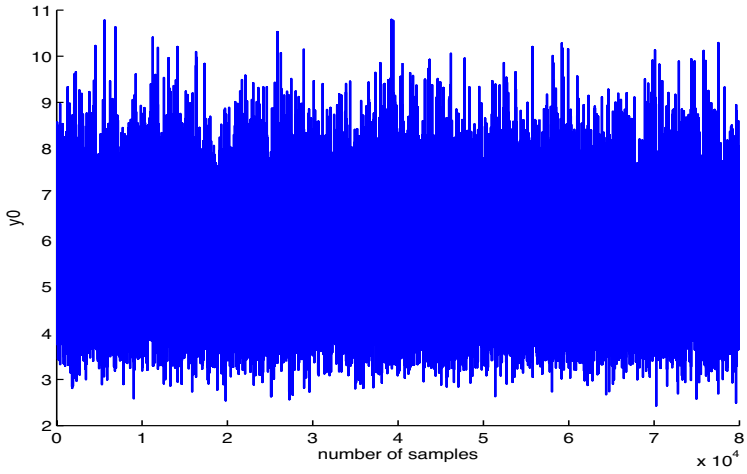

Figure 4.6: Chains convergent for SIV model parameter y_0 for untreated macaques

4.C Numerical Results

4.C.1 Parameter estimates

The fitted parameter estimates for β_ϵ and y_0 are located in Table 4.3.

Datasets	Symbol	Parameter	Distribution	Estimate (95% Credible Interval)	Unit
HIV-1 without neuro-logical disorders	y_0	Initial number of infected brain macrophages	U(0.1, 2)	0.1-2	per g
	β_ϵ	Transmission coefficient	U(10^{-8}, 10^{-6})	6.72-7.60$\times10^{-7}$	per year
HIV-1 with neuro-logical disorders	y_0	Initial number of infected brain macrophages	U(0.1, 2)	0.1-2	per g
	β_ϵ	Transmission coefficient	U(10^{-8}, 10^{-5})	7.89-8.78$\times10^{-7}$	per year
SIV untreated	y_0	Initial number of infected brain macrophages	U(0, 90.19)	5.45 (4.20, 6.99)	per g
	β_0	Transmission coefficient	U(10^{-8}, 10^{-4})	5.98$\times10^{-6}$ (5.62×10^{-6}, 6.35×10^{-6})	per year

Table 4.3: Fitted parameter estimates and assumed distributions for the model fit to three datasets.

The unnormalized posterior distribution for each estimated parameter are displayed in Figures 4.7, 4.8, 4.9, 4.10, 4.11, and 4.12.

In Figures 4.7, 4.8, 4.9, 4.10, it is seen that the unnormalized posterior distributions for the estimated parameters are flat for the data corresponding to cART-treated HIV-1 infected patients without neurological disorders and with neurological disorders. This occurs because the model is fit to only one data point at 10 years from primary infection for the two datasets (Table 2.1). In Figures 4.8 and 4.10, it is observed that the range from 0.1-2 is equally likely for

y_0 because there is only one data point at 10 years from primary infection and the prior of y_0 is U(0.1, 2). The prior for β_ϵ is U$(10^{-8}, 10^{-5})$. Given the single data point at 10 years from primary infection and $y_0 \sim$ U(0.1, 2), it is seen in Figures 4.7 and 4.9 that the range of β_ϵ is equally likely and restricted between 6.72-7.60$\times 10^{-7}$ for cART-treated patients without neurological disorders and 7.89-8.78$\times 10^{-7}$ for cART-treated patients with neurological disorders.

In Figures 4.11 and 4.12, the unnormalized posterior distributions for the estimated parameters are symmetric and unimodal for the data corresponding to untreated SIV-infected macaques. This happens because the model is fit to multiple data points for the dataset (Table 2.1). In Figure 4.11, it is seen that the unnormalized posterior distribution for β_ϵ has a most likely point estimate of 5.98$\times 10^{-6}$ and has a 95% Bayesian credible interval of 5.62-6.35$\times 10^{-6}$. In Figure 4.12, it is observed that the unnormalized posterior distribution for y_0 has a most likely point estimate of 5.45 and has a 95% Bayesian credible interval of 4.20-6.99.

4.C.2 HIV-infected brain macrophage burden

For cART-treated HIV/AIDS patients without neurological disorders, it would require 37-95 years to reach the set point of 3.64-7.08$\times 10^5$ infected brain macrophages per gram (brain tissue). In contrast, among cART-treated HIV/AIDS patients with comorbid neurological disorders (HAND or HIVE), 20-37 years would be necessary to establish the set point of 0.805-1.06$\times 10^6$ infected brain macrophages per gram (brain tissue). The HIV-1 infected brain macrophage burden for patients without neurological disorders and with neurological disorders is displayed in Fig. 4.13 (A) and 1(B), respectively.

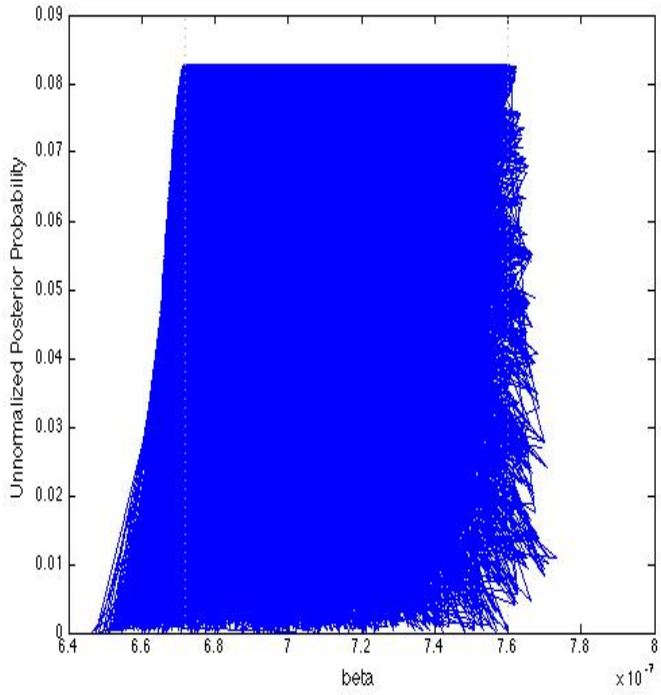

Figure 4.7: Posterior for HIV model parameter β for cART-treated patients without neurological disorders

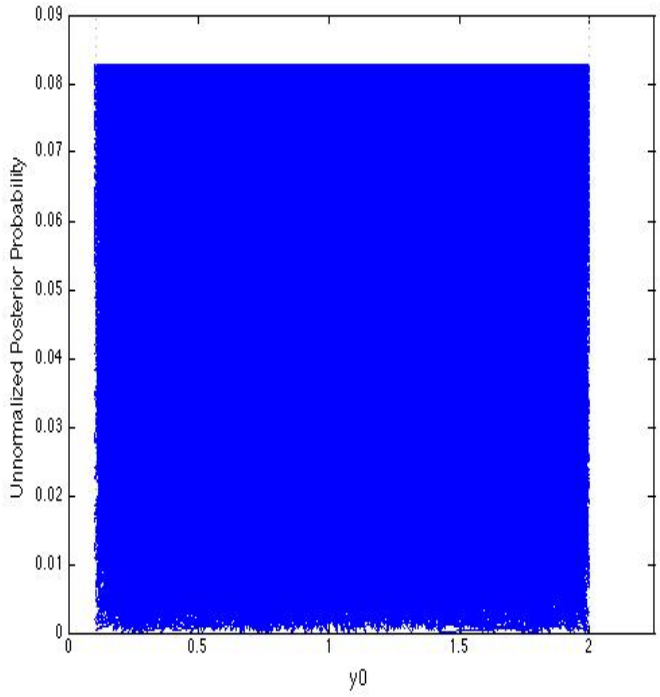

Figure 4.8: Posterior for HIV model parameter y_0 for cART-treated patients without neurological disorders

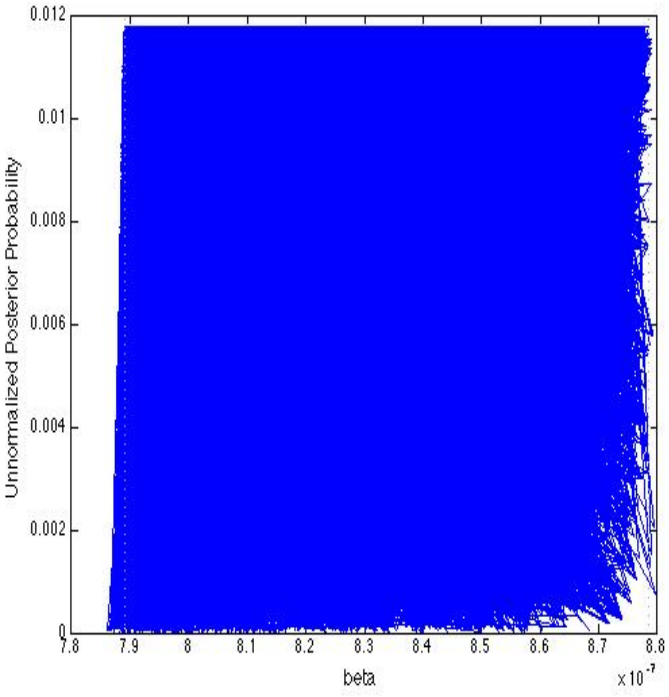

Figure 4.9: Posterior for HIV model parameter β for cART-treated patients with neurological disorders

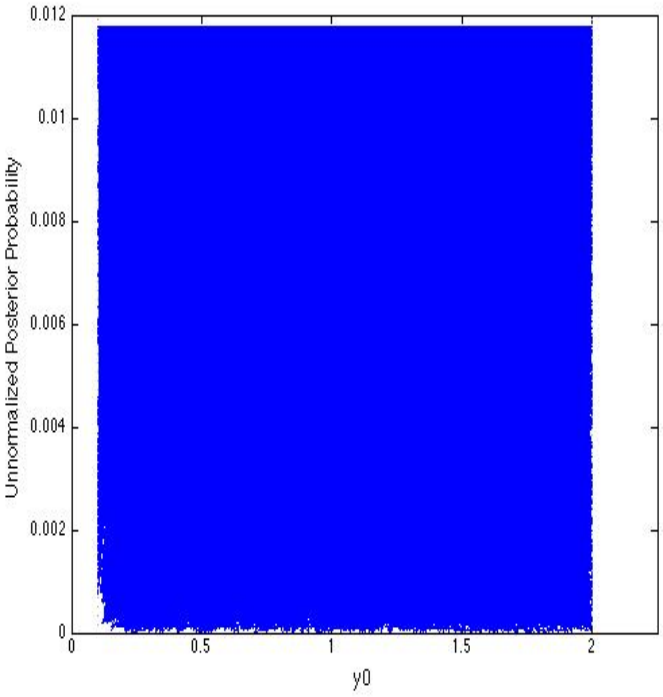

Figure 4.10: Posterior for HIV model parameter y_0 for cART-treated patients with neurological disorders

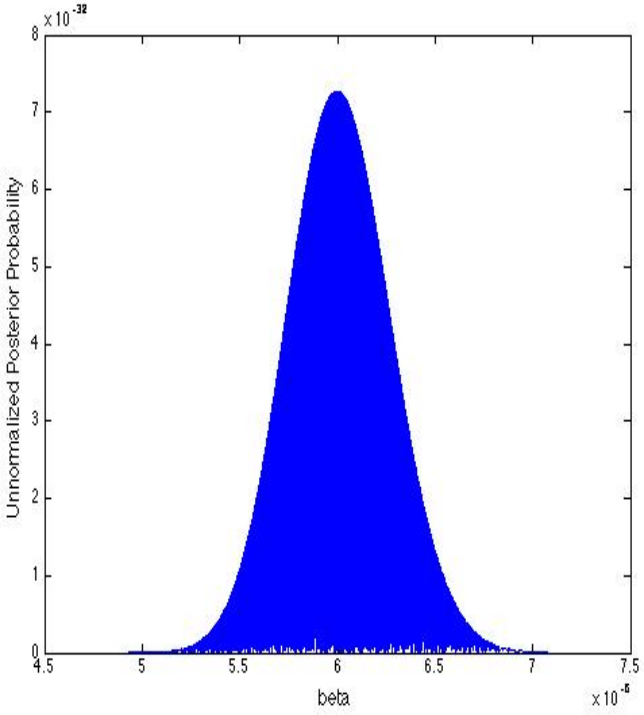

Figure 4.11: Posterior for SIV model parameter β for untreated macaques

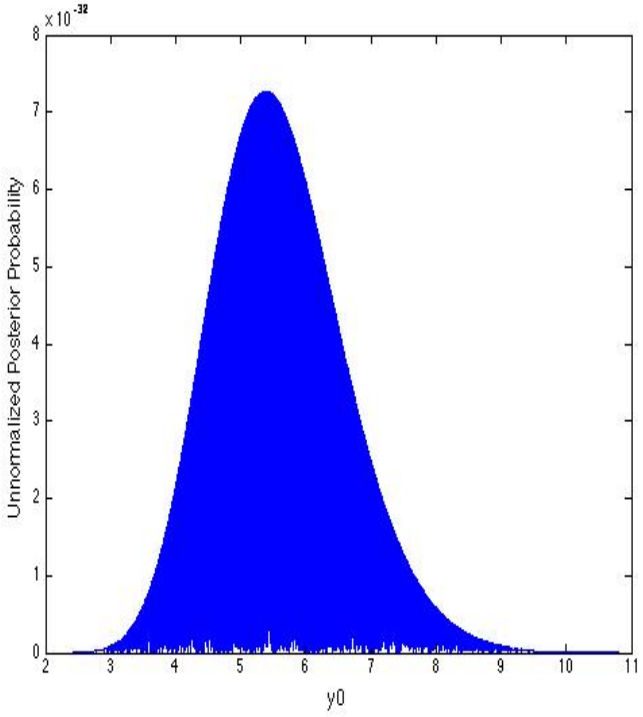

Figure 4.12: Posterior for SIV model parameter y_0 for untreated macaques

4.C.3 SIV-infected brain macrophage burden

For untreated SIV-infected macaques, it would require approximately 1.5 years to meet the set point of 3.00×10^6 infected brain macrophages per gram (brain tissue). SIV-infected brain macrophage burden for untreated macaques is shown in Fig. 4.13 (C).

4.C.4 Comparison of transmission rates

The estimated values of the transmission coefficient β_ϵ in Table 4.3 were used to compare the viral transmission rates in brain for the three study cohorts. The HIV-1 transmission rate was 1.04-1.31 times higher for cART-treated HIV-infected patients with neurological disorders compared to those without neurological disorders. The transmission rate for SIV infection among untreated macaques was 6.40-9.45 times faster compared to cART-treated HIV-1 patients. When compared to the transmission coefficient for HIV-1 infection in the plasma in the literature [58], we found that the HIV-1 transmission rate among CD4+ T cells was 2.2-3.9 log_{10} fold higher than HIV-1 infection among brain macrophages. These findings suggest the progression of HIV-1 infection in the brain was slower in comparison to HIV-1 infection in the plasma [58].

4.C.5 Minimum cART improvement to inhibit replication

For untreated SIV-infected macaques the estimated baseline R_0 value was 9.38-10.60. In the literature, the R_0 value for untreated SIV-infected macaques in the plasma has a range of 2-68 [59]. For the infection to decline in the brain for untreated SIV-infected macaques it is necessary to have $\epsilon > 0$. To inhibit

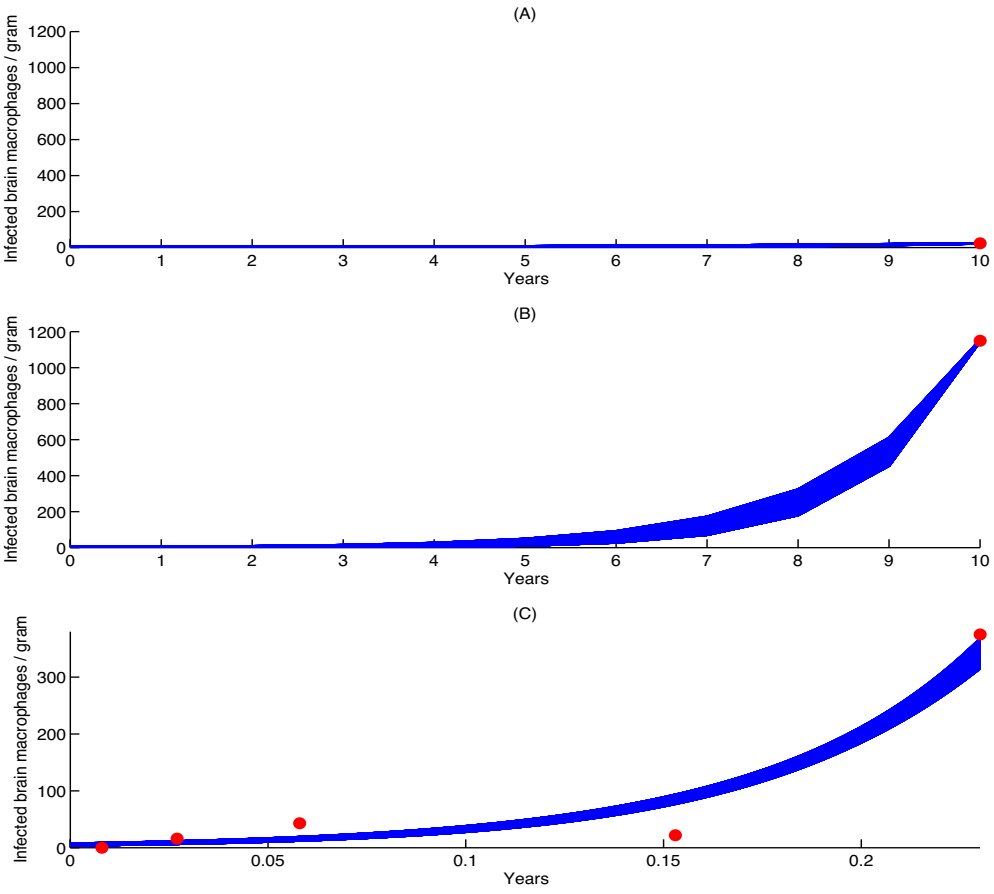

Figure 4.13: Infected brain macrophage burden.

(A) cART-treated HIV-infected patients without neurological disorders. (B) cART-treated HIV-infected patients with neurological disorders. (C) SIV-infected (untreated) macaques. Curves lying in the blue region represent the most likely model solutions for the mean given the data point(s) in red.

replication in the brain for untreated SIV-infected macaques, we require that $R_\epsilon < 1$ and the minimum cART effectiveness ϵ was estimated to be 89.35-90.57%.

For cART-treated patients without neurological disorders the estimated baseline R_ϵ value was 1.12-1.27. The estimated baseline value of R_ϵ was 1.32-1.47 for cART-treated patients with neurological disorders. In comparison, the R_0 value for untreated HIV-1 infection in the plasma has median 8.0 and interquartile range 4.9-11 [60]. In the literature, a cART effectiveness of 0.85 would suppress the viral load in the plasma to undetectable levels after a few months of treatment [15]. Using a cART effectiveness of 0.85 [15] and the R_0 value for untreated HIV-1 infection in the plasma with range 4.9-11 [60], the value of $R_{0.85}$ for treated HIV-1 infection in the plasma would be in the range 0.74-1.65. The estimated value of R_ϵ in the brain for cART-treated patients was found to range from 1.12-1.47 and lies in the range 0.74-1.65.

To inhibit replication in the brain, the minimum improvement in cART effectiveness from the estimated baseline was determined to be 10.71-21.26% for patients without neurological disorders, and 24.24-31.97% for patients with neurological disorders.

4.C.6 50% improvement cART late presenter

Provided cART suppresses HIV-1 infection outside the brain, and with a 50% improvement in cART efficiency from the estimated baseline in the brain, it would require 9-11 years to reduce the level of infected brain macrophages to approximately 0.001 per gram for a late diagnosed patient without neurological disorders, and it would require 20-26 years for the same reduction for a late

diagnosed patient with neurological disorders (Fig. 4.14 (A) and 4.14 (B) respectively).

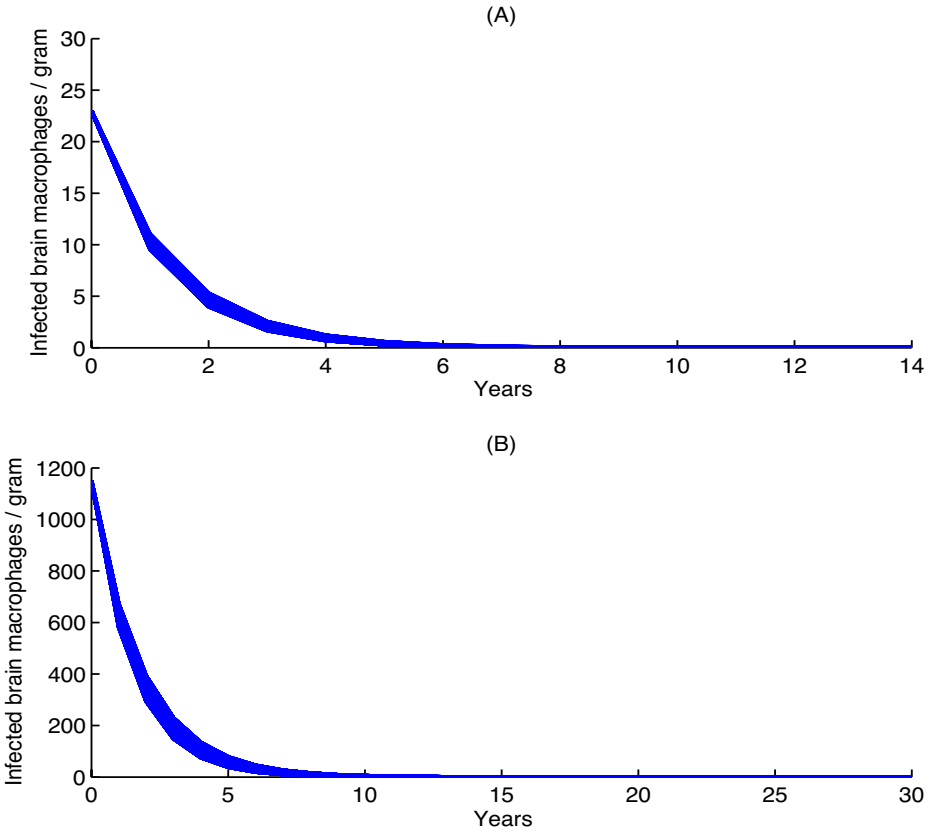

Figure 4.14: HIV-1 infected brain macrophage burden with cART.

Assuming a 50% improved efficiency in cART. (A) Late presenting patients without neurological disorders and (B) late presenting patients with neurological disorders will show differing durations to the time of eradication. Curves lying in the blue region represent the most likely model solutions for the mean.

Chapter 5

Discussion and conclusions

5.A Discussion

We focused on brain viral DNA as a marker of infected cells in contrast to brain viral RNA. Brain viral RNA levels varied widely over time [32, 31, 33, 34, 35]. Brain viral DNA levels displayed less variability and were determined to be a stable indicator of infection. We used the study of a single HIV-infected patient to gain insight into the state of brain infection during the eclipse phase; 15 days after iatrogenic HIV-1 infection, HIV-1 was detected in the brain [16]. We also relied on data from a study examining human brain specimens from the NNTC; these data provided findings from patients with advanced disease [31]. This latter study reported that brain viral RNA was higher in patients with neurological disorders, HAND and HIVE, than patients without neurological disorders and that brain viral RNA and DNA levels were correlated with worse neuropsychological performance [31]. A study not included in our research was a paper examining the brain viral DNA and brain viral RNA of 15 patients [61]. In this study, there was no significant difference in brain viral DNA between

patients with and without neurological disorders [61]. This result is later contradicted by a study examining a larger sample size of 195 patients [31]. A paper also not included in our research examined the brain viral DNA levels of 17 HIV-1 infected asymptomatic patients and 16 HIV-1 infected patients with AIDS [62]. This paper found that the brain viral DNA levels of AIDS patients were found to be higher than those HIV-1 infected asymptomatic patients [62]. This paper was not included in our study due to the small sample of patients [62]. Lastly, another study not included in our research examined brain viral RNA and DNA levels of 21 patients with 9 patients having neurological disorders [63]. This study found that the mean of the viral load was larger for patients with neurological disorders than those patients without neurological disorders but this did not reach the appropriate statistical level [63]. The larger sample size of 195 patients in the later study determines that the RNA and DNA viral load is significantly larger for patients with neurological disorders than patients without neurological disorders [31].

In blood-derived lymphocytes, the average ratio of integrated proviral DNA to total viral DNA is 1:86 [39]. We used this ratio as an estimate for the average ratio of integrated proviral DNA to total viral DNA in brain macrophages. An earlier study found the ratio of integrated proviral DNA to total viral DNA in brain tissues from HIV-1 encephalitis cases ranged from 1:6 to 1:81 [64]. The average ratio in blood and the ratio in brain tissues from HIV-1 encephalitis patients are the same order of magnitude. In the present study, changing this ratio of integrated proviral DNA to total viral DNA would affect the estimated mean integrated viral DNA copies per gram of brain tissue used to fit the mathematical model. In the extreme case of 1:6 being the ratio of integrated proviral DNA to total viral DNA, there was an estimated 8-

12% difference between the new transmission coefficient and the transmission coefficient estimated under the ratio assumption of 1:86.

Brain tissue measurements from a HIV-1 infected patient are very rarely available before death. Two major limitations in using autopsy data for brain tissue from human cohorts are minimal knowledge regarding durations of infection and antiretroviral therapy for each patient. An estimate for the duration of infection for each patient in the autopsy data assumes each patient has AIDS and died at least 10 years after primary infection whether or not a patient is active on antiretroviral therapy within 1 year of death. An issue not addressed herein is viral burden in CSF; many studies have reported on HIV-1 RNA levels in CSF, albeit free virus particles [65]. CSF as an indicator of viral dynamics within brain has substantial challenges because the relative paucity of cells in CSF compounded by the predominance of lymphocytes in CSF, presumably derived from blood, making it a questionable surrogate indicator of brain virus-related events. However, it would be valuable to have a better understanding of brain-CSF correlations in viral replication and latency in the future management of patients receiving cART.

The obstacles described in obtaining accurate estimates of the durations of infection and antiretroviral therapy for individual patients necessitates the use of SIV studies where the durations of infection and antiretroviral therapy for each macaque are known. Most of our SIV data comes from the same animal model [32, 33, 34]. Thus, the present SIV results may be specific to this animal model. We used published experimental data from four SIV studies that examined macaque brains at different times post-infection (p.i.) [32, 33, 34, 35]. The earliest SIV study used in the present analyses showed that total viral DNA was not detected in the brain at 3 days p.i. but viral

DNA was detected on all subsequent time points (7, 14, 21, 50 days p.i.) [35]. Another SIV study found that brain viral DNA levels remained at constant levels from the acute phase through the asymptomatic period [33]. A further SIV study demonstrated that cART was capable of reducing brain viral RNA to undetectable levels but had little impact on brain viral DNA levels after acute infection [32]. The last included SIV study reported that cART greatly reduced viral RNA levels, but exerted little effect on viral DNA levels at 21 days p.i. [34]. The current mathematical investigations indicated that the mathematical model adequately fits the experimental in vivo SIV data. This modeling strategy could be applied to SIV datasets from other animal models, yielding insights into the viral progression rate in brain macrophages from primary infection.

A 0.85 cART effectiveness would suppress the viral load in the plasma to undetectable levels after a few months of treatment [15]. If cART effectiveness was 0.85 within the brain ($\epsilon = 0.85$), the R_0 value in the brain for untreated patients would be in the range 7.47-9.80, similar to the R_0 range for untreated HIV-1 infection in the plasma 4.9-11. Yet the blood-brain barrier restricts some antiretroviral agents from entering the brain [5] and a 0.85 cART effectiveness in the brain would most likely be too large a value. If cART effectiveness was less than 0.85 ($\epsilon < 0.85$), the small value of R_ϵ in the brain for cART-treated patients 1.12-1.47 might be due to a slower progression of HIV-1 infection in the brain in comparison to HIV-1 infection in the plasma.

Because of the limited data available for HIV-1 and SIV brain infection it was necessary to use a simple mathematical model that restricted the number of model parameters needed to fit the empiric data. Although microglia and trafficking macrophages might behave differently, these cell populations were

treated as the single cell population of brain macrophages. Although astrocytes constitute a large proportion of cells in the human brain, astrocytes were not considered in this study because astrocytes have a limited infection and produce little or no virus [42]. Different anatomical areas within the brain contain variable levels of HIV-1 and SIV infected cells during disease progression [66]. In this model it is assumed that the infected brain macrophage population is distributed homogeneously across the entire brain; moreover, an infected brain macrophage might be productively or latently infected. The model does not make this distinction for infected brain macrophages. Despite these simplifications our model provides an estimate of the HIV-infected brain macrophage burden from primary infection and the necessary improvements in current cART regimens needed to curtail and eventually eliminate HIV-1 infection from the brain.

5.B Conclusions and further directions

To our knowledge this is the first mathematical modeling study to quantify HIV-1 and SIV infection dynamics in the brain. Our modeling study indicates that HIV-1 and SIV provirus burdens in brain increase slowly over time. Assuming antiretroviral therapy suppresses HIV-1 infection outside the brain, an effective antiretroviral therapy could eradicate HIV-1 infection in the brain, albeit over a decade for patients without neurological complications and over two decades for those with HAND.

Future studies are warranted to model both productively and latently infected brain macrophages using the viral DNA and viral RNA data. This approach would allow a more accurate estimation of cART effectiveness. The

application of HIV-infected humanized mice with and without cART might facilitate this effort [67]. Creating a model to quantify viral infection in specific areas of the brain over time would also be informative, as it would permit determination of which regions of the brain display the largest viral burden over the course of infection and how cART might be optimized to ensure rapid eradication of virus from the brain.

Bibliography

[1] R. Lorenzo-Redondo, H. R. Fryer, T. Bedford, E. Y. Kim, J. Archer, S. L. K. Pond, and et al, "Persistent hiv-1 replication maintains the tissue reservoir during therapy," *Nature*, vol. doi:10.1038/nature16933, 2016.

[2] S. G. Deeks, J. Overbaugh, A. Phillips, and S. Buchbinder, "Hiv infection," *Nat Rev Dis Primers*, vol. 1, pp. 1–22, 2015.

[3] C. D. Pilcher, D. C. Shugars, S. A. Fiscus, W. C. Miller, P. Menezes, J. Giner, and et al, "Hiv in body fluids during primary hiv infection: implications for pathogenesis, treatment and public health," *AIDS*, vol. 15, pp. 837–845, 2001.

[4] A. Nath, "Eradication of human immunodeficiency virus from brain reservoirs," *J Neurovirol*, vol. 21, pp. 227–234, 2015.

[5] L. Annamalai, V. Bhaskar, D. R. Pauley, H. Knight, K. Williams, M. Lentz, and et al, "Impact of short-term combined antiretroviral therapy on brain virus burden in simian immunodeficiency virus-infected and cd8+ lymphocyte-depleted rhesus macaques," *Am J Pathol*, vol. 177, no. 2, pp. 777–791, 2010.

[6] S. Spudich and F. González-Scarano, "Hiv-1-related central nervous system disease: Current issues in pathogenesis, diagnosis, and treatment," *Cold Spring Harb Perspect Med*, vol. 2, no. 6, p. a007120, 2012.

[7] P. Vivithanaporn, G. Heo, J. Gamble, H. B. Krentz, A. Hoke, M. J. Gill, and et al, "Neurologic disease burden in treated hiv/aids predicts survival," *Neurology*, vol. 75, pp. 1150–1158, 2010.

[8] M. K. Patrick, J. B. Johnston, and C. Power, "Lentiviral neuropathogenesis: comparative neuroinvasion, neurotropism, neurovirulence, and host neurosusceptibility," *J Virol*, vol. 76, no. 16, pp. 7923–7931, 2002.

[9] M. A. Nowak and R. M. May, *Virus dynamics. Mathematical principles of immunology and virology.* Oxford: Oxford University Press, 2000.

[10] D. E. Kirschner and A. S. Perelson, *A model for the immune system response to HIV: AZT treatment studies. In: Mathematical population dynamics: analysis of heterogeneity, vol. 1, theory of epidemics*. Winnipeg: Wuerz Publishing Ltd, 1995.

[11] M. J. Kuroda, "Macrophages: do they impact aids progression more than cd4 t cells?," *J Leukoc Biol*, vol. 87, no. 4, pp. 569–573, 2010.

[12] B. M. Peterlin and D. Trono, "Hide, shield and strike back: How hiv-infected cells avoid immune eradication," *Nat Rev Immunol*, vol. 3, pp. 97–107, 2003.

[13] A. Perelson and R. M. Ribeiro, "Modeling the within-host dynamics of hiv infection," *BMC Biol*, vol. 11, no. 96, 2013.

[14] D. Wodarz and M. A. Nowak, "Mathematical models of hiv pathogenesis and treatment," *Bioessays*, vol. 24, no. 12, pp. 1178–1187, 2002.

[15] L. Rong and A. S. Perelson, "Modeling latently infected cell activation: viral and latent reservoir persistence, and viral blips in hiv-infected patients on potent therapy," *PLoS Comput Biol*, vol. 5, no. 10, p. e1000533, 2009.

[16] L. E. Davis, B. L. Hjelle, V. E. Miller, D. L. Palmer, A. L. Llewellyn, T. L. Merlin, and et al, "Early viral brain invasion in iatrogenic human immunodeficiency virus infection," *Neurology*, vol. 42, pp. 1736–1739, 1992.

[17] K. W. Witwer, L. Gama, M. Li, C. M. Bartizal, S. E. Queen, J. J. Varrone, and et al, "Coordinated regulation of siv replication and immune responses in the cns," *PLoS One*, vol. 4, no. 12, p. e8129, 2009.

[18] F. González-Scarano and J. Martin-Garcia, "The neuropathogenesis of aids," *Nat Rev Immunol*, vol. 5, pp. 69–81, 2005.

[19] J. H. Campbell, E. M. Ratai, P. Autissier, D. J. Nolan, S. Tse, A. D. Miller, and et al, "Anti-4 antibody treatment blocks virus traffic to the brain and gut early, and stabilizes cns injury late in infection," *PLoS Pathog*, vol. 10, no. 12, pp. 1–15, 2014.

[20] K. A. Lindl, D. R. Marks, and D. L. Kolson, "Hiv-associated neurocognitive disorder: pathogenesis and therapeutic opportunities," *J Neuroimmune Pharmacol*, vol. 5, pp. 294–309, 2010.

[21] Q. Li, F. Lu, and K. Wang, "Modeling of hiv-1 infection: Insights to the role of monocytes/macrophages, latently infected t4 cells, haart regimes," *PLoS One*, 2012.

[22] M. Joly and J. M. Pinto, "An in-depth analysis of the hiv-1/aids dynamics by comprehensive mathematical modeling," *Math Comput Model*, 2011.

[23] M. Valle, R. W. Price, A. Nilsson, M. Heyes, and D. Verotta, "Csf quinolinic acid levels are determined by local hiv infection: cross-sectional analysis and modelling of dynamics following antiretroviral therapy," *Brain*, vol. 127, no. 1047-1060, 2004.

[24] J. L. Spouge, R. I. Shrager, and D. S. Dimitrov, "Hiv-1 infection kinetics in tissue cultures," *Math Biosci*, vol. 138, pp. 1–22, 1996.

[25] R. V. Culshaw, S. Ruan, and G. Webb, "A mathematical model of cell-to-cell spread of hiv-1 that includes a time delay," *J Math Biol*, vol. 46, pp. 425–444, 2003.

[26] M. Kouche and B. Ainseba, "A mathematical model of hiv-1 infection including the saturation effect of healthy cell proliferation," *Int J Appl Math Comput Sci*, vol. 20, no. 3, pp. 601–612, 2010.

[27] T. Hastie, R. Tibshirani, and J. Friedman, *The Elements of Statistical Learning: Data Mining, Inference, and Prediction*. Springer Science+Business Media, LLC, 2009.

[28] M. Dunbar, J. M. Murray, L. A. Cysique, B. J. Brew, and V. Jeyakumar, "Simultaneous classification and feature selection via convex quadratic programming with application to hiv-associated neurocognitive disorder assessment," *Eur J Oper Res*, vol. 206, pp. 470–478, 2010.

[29] L. A. Cysique, J. M. Murray, M. Dunbar, V. Jeyakumar, and B. J. Brew, "A screening algorithm for hiv-associated neurocognitive disorders," *HIV Med*, vol. 11, pp. 642–649, 2010.

[30] S. L. Lamers, G. B. Fogel, D. J. Nolan, M. S. McGrath, and S. Marco, "Hiv-associated neuropathogenesis: A systems biology perspective for modeling and therapy," *Biosystems*, vol. 119, pp. 53–61, 2014.

[31] B. B. Gelman, J. G. Lisinicchia, S. Morgello, E. Masliah, D. Commins, C. L. Achim, and et al, "Neurovirological correlation with hiv-associated neurocognitive disorders and encephalitis in a haart-era cohort," *J Acquir Immune Defic Syndr*, vol. 62, no. 5, pp. 487–495, 2013.

[32] M. C. Zink, A. K. Brice, K. M. Kelly, S. E. Queen, L. Gama, M. Li, and et al, "Simian immunodeficiency virus-infected macaques treated with highly active antiretroviral therapy have reduced central nervous system viral replication and inflammation but persistence of viral dna," *J Infect Dis*, vol. 202, no. 1, pp. 161–170, 2010.

[33] J. E. Clements, T. Babas, J. L. Mankowski, K. Suryanarayana, M. P. Jr., P. M. Tarwater, and et al, "The central nervous system as a reservoir for simian immunodeficiency virus (siv): steady-state levels of siv dna in brain from acute through asymptomatic infection," *J Infect Dis*, vol. 186, pp. 905–913, 2002.

[34] D. Graham, L. Gama, S. E. Queen, M. Li, A. K. Brice, K. M. Kelly, and et al, "Initiation of haart during acute simian immunodeficiency virus infection rapidly controls virus replication in the cns by enhancing immune activity and preserving protective immune responses," *J Neurovirol*, vol. 17, pp. 120–130, 2011.

[35] K. C. Williams, S. Corey, S. V. Westmoreland, D. Pauley, H. Knight, C. deBakker, and et al, "Perivascular macrophages are the primary cell type productively infected by simian immunodeficiency virus in the brains of macaques: implications for the neuropathogenesis of aids," *J Exp Med*, vol. 193, no. 8, pp. 905–915, 2001.

[36] F. A. C. Azevedo, L. R. B. Carvalho, L. T. Grinberg, J. M. Farfel, R. E. L. Ferretti, R. E. P. Leite, and et al, "Equal numbers of neuronal and non-neuronal cells make the human brain an isometrically scaled-up primate brain," *J Comp Neurol*, vol. 513, pp. 532–541, 2009.

[37] S. Herculano-Houzel, "The glia/neuron ratio: how it varies uniformly across brain structures and species and what that means for brain physiology and evolution," *Glia*, vol. 62, pp. 1377–1391, 2014.

[38] P. Hartmann, A. Ramseier, F. Gudat, M. J. Mihatsch, and W. Polasek, "Normal weight of the brain in adults in relation to age, sex, body height and weight," *Pathologe*, vol. 15, no. 3, pp. 165–170, 1994.

[39] R. Suspène and A. Meyerhans, "Quantification of unintegrated hiv-1 dna at the single cell level in vivo," *PLoS One*, vol. 7, no. 5, p. e36246, 2012.

[40] T. B. P. L. (unpublished).

[41] R. K. Fujimura, P. Shapshak, D. Feaster, M. Epler, and K. Goodkin, "A rapid method for comparative quantitative polymerase chain reaction of hiv-1 proviral dna extracted from cryopreserved brain tissues," *J Virol Methods*, vol. 67, pp. 177–187, 1997.

[42] L. R. Gray, S. G. Turville, T. L. Hltchen, W. J. Cheng, A. M. Ellett, H. Salimi, and et al, "Hiv-1 entry and trans-infection of astrocytes involves cd81 vesicles," *PLoS One*, vol. 9, no. 2, p. e90620, 2014.

[43] J. G. Walsh, S. N. Reinke, M. K. Mamik, B. A. McKenzie, F. Maingat, W. G. Branton, and et al, "Rapid inflammasome activation in microglia contributes to brain disease in hiv/aids," *Retrovirology*, vol. 11, no. 35, 2014.

[44] D. Wodarz, M. A. Nowak, and C. R. Bangham, "The dynamics of htlv-i and the ctl response," *Immunol Today*, vol. 20, no. 5, pp. 220–227, 1999.

[45] H. Gómez-Acevedo, M. Y. Li, and S. Jacobson, "Multistability in a model for ctl response to htlv-i infection and its implications to ham/tsp development and prevention," *Bull Math Biol*, vol. 72, no. 3, pp. 681–696, 2010.

[46] L. Perko, *Differential Equations and Dynamical Systems*. Springer-Verlag New York, Inc., second edition ed., 1991.

[47] J. L. Willems, *Stability Theory of Dynamical Systems*. Thomas Nelson and Sons LTD., 1970.

[48] W. A. Coppel, *Stability and Asymptotic Behavior of Differential Equations*. D. C. Heath and Company, 1965.

[49] T. M. Inc. Matlab version 8.3.0.532 Natick, Massachusetts., 2014.

[50] A. Grinsted, "Markov chain monte carlo sampling of posterior distribution." http://www.mathworks.com/matlabcentral/fileexchange/49820-grinsted-gwmcmc, 2015.

[51] L. J. Bain and M. Engelhardt, *Introduction to Probability and Mathematical Statistics*. Brooks/Cole, second edition ed., 1987.

[52] C. E. Rasmussen and C. K. I. Williams, *Gaussian Processes for Machine Learning*. MIT Press, 2006.

[53] V. Periwal, C. C. Chow, R. N. Bergman, M. Ricks, G. L. Vega, and A. E. Sumner, "Evaluation of quantitative models of the effect of insulin on lipolysis and glucose disposal," *Am J Physiol Regul Integr Comp Physiol*, vol. 295, pp. R1089–R1096, 2008.

[54] J. G. Kalbfleisch, *Probability and Statistical Inference*, vol. Volume 2: Statistical Inference. Springer-Verlag New York, Inc., 1979.

[55] Y. Z. Ma and A. Berndsen, "How to combine correlated data sets - a bayesian hyperparameter matrix method," *Astronomy and Computing*, vol. 5, pp. 45–56, 2014.

[56] R. Durrett, *Probability: Theory and Examples*. Brooks/Cole-Thomson Learning, third edition ed., 2005.

[57] A. Gelman and S. P. Brooks, "General methods for monitoring convergence of iterative simulations," *J Comp Graph Stat*, vol. 7, no. 4, pp. 434–455, 1998.

[58] C. L. Althaus, B. Joos, A. S. Perelson, and H. F. Günthard, "Quantifying the turnover of transcriptional subclasses of hiv-1-infected cells," *PLoS Comput Biol*, vol. 10, no. 10, p. e1003871, 2014.

[59] M. A. Nowak, A. L. Lloyd, G. M. Vasquez, T. A. Wiltrout, L. M. Wahl, N. Bischofberger, and et al, "Viral dynamics of primary viremia and antiretroviral therapy in simian immunodeficiency virus infection," *J Virol*, vol. 71, no. 10, pp. 7518–7525, 1997.

[60] R. M. Ribeiro, L. Qin, L. L. Chavez, D. Li, S. G. Self, and A. S. Perelson, "Estimation of the initial viral growth rate and basic reproductive number during acute hiv-1 infection," *J Virol*, vol. 84, no. 12, pp. 6096–6102, 2010.

[61] R. T. Johnson, J. D. Glass, J. C. McArthur, and B. W. Chesebro, "Quantitation of human immunodeficiency virus in brains of demented and nondemented patients with acquired immunodeficiency syndrome," *Ann Neurol*, vol. 39, no. 3, pp. 392–395, 1996.

[62] S. F. An, B. Giometto, and F. Scaravilli, "Hiv-1 dna in brains in aids and pre-aids: Correlation with the stage of disease," *Ann Neurol*, vol. 40, pp. 611–617, 1996.

[63] F. Lazarini, D. Seilhean, O. Rosenblum, S. Suarez, L. Conquy, T. Uchinhara, V. Sazdovitch, K. Mokhtari, T. Maisonobe, F. Boussin, C. Katlama, F. Bricaire, C. Duyckaerts, and J. J. Hauw, "Human immunodeficiency virus type 1 dna and rna load in brains of demented and nondemented patients with acquired immunodeficiency syndrome," *J Neurovirol*, vol. 3, pp. 299–303, 1997.

[64] S. Pang, Y. Koyanagi, S. Miles, C. Wiley, H. V. Vinters, and I. S. Y. Chen, "High levels of unintegrated hiv-1 dna in brain tissue of aids dementia patients," *Nature*, vol. 343, no. 6253, pp. 85–89, 1990.

[65] S. Nightingale, A. Winston, S. Letendre, B. D. Michael, J. C. McArthur, S. Khoo, and et al, "Controversies in hiv-associated neurocognitive disorders," *Lancet Neurol*, vol. 13, no. 11, pp. 1139–1151, 2014.

[66] K. Kure, K. M. Weidenheim, W. D. Lyman, and D. W. Dickson, "Morphology and distribution of hiv-1 gp41-positive microglia in subacute aids encephalitis. pattern of involvement resembling a multisystem degeneration," *Acta Neuropathol*, vol. 80, pp. 393–400, 1990.

[67] M. Araínga, S. Hang, L. Y. Poluektova, S. Gorantla, and H. E. Gendelman, "Hiv-1 cellular and tissue replication patterns in infected humanized mice," *Sci Rep*, vol. 6, no. 23513, 2016.